17449

NATIONAL LIBRARY
OTTAWA

CANADA

BIBLIOTHÈQUE NATIONALE
OTTAWA

NAME OF AUTHOR.....STEPHAN BEHAN.....

TITLE OF THESIS...EXPERIMENTAL INVESTIGATION OF PULSATILE BLOOD FLOW THROUGH THE LARGE CURVE BIFURCATION...

UNIVERSITY.....THE UNIVERSITY OF ALBERTA.....

DEGREE FOR WHICH THESIS WAS PRESENTED.....M.Sc.....

YEAR THIS DEGREE GRANTED.....1973.....

Permission is hereby granted to THE NATIONAL LIBRARY OF CANADA to microfilm this thesis and to lend or sell copies of the film.

The author reserves other publication rights, and neither the thesis nor extensive extracts from it may be printed or otherwise reproduced without the author's written permission.

(Signed).....S. Behan.....

PERMANENT ADDRESS:

143 - 3rd AV. S.E.

MEDICINE HAT

ALBERTA - CANADA

DATED.....October 4.....1973

NL-91 (10-68)

THE UNIVERSITY OF ALBERTA

EXPERIMENTAL INVESTIGATION OF THE BLOOD FLOW CHARACTERISTICS IN THE AORTIC ARCH

BY

© STEPHAN BEHAN

A THESIS

SUBMITTED TO THE FACULTY OF GRADUATE STUDIES

IN PARTIAL FULFILMENT OF THE REQUIREMENTS FOR THE DEGREE

OF MASTER OF SCIENCE

DEPARTMENT OF MECHANICAL ENGINEERING

EDMONTON, ALBERTA

FALL, 1973

THE UNIVERSITY OF ALBERTA

FACULTY OF GRADUATE STUDIES

The undersigned certify that they have read, and recommend to the Faculty of Graduate Studies for acceptance, a thesis entitled "EXPERIMENTAL INVESTIGATION OF THE BLOOD FLOW CHARACTERISTICS IN THE AORTIC ARCH" submitted by Stephan Behan in partial fulfilment of the requirements for the degree of Master of Science.

A Rodbiewicz
Supervisor

J D Dale

H Seyer

H Rutherford

Date 24th Sept 73

ABSTRACT

An experimental investigation is presented for both steady and pulsatile flow of blood through the aorta. A mixture of glycerine and water was used as a blood model. The effect of varying the significant parameters, Reynolds Number, Re, unsteadiness parameter, α, and normalized velocity fluctuation, λ, is revealed through their influence on the mass flow ratios; the mass flow ratios γ_n(n=1, 2, 3, 4, 5) being the ratios of the mass flows in the right subclavian, right carotid, left carotid, left subclavian and thoracic aorta, respectively, to the total mass flow.

An experimental apparatus and an artificial aorta were designed and constructed to simulate the physiological range of these parameters. One type of rigid artificial aorta was examined.

For pulsatile flow, γ_1 was found to be independent of the unsteadiness parameter, α, in the range $10 \leq \alpha \leq 20$, and was found to be a decreasing function in the lowest range $8 \leq \alpha \leq 10$. Furthermore, γ_1 was found to be a decreasing function of both the Reynolds Number and the normalized velocity fluctuation up to the range of Re = 1500. For larger Re, as for steady flow, γ_1, is a decreasing function of Re only.

The mass flow ratio, γ_2, showed the same dependence as γ_1 except that it was more strongly influenced by Re and not as strongly influenced by the normalized velocity fluctuation. The mass flow ratio, γ_3, showed the same dependence as γ_1. The mass flow ratio, γ_4, was similarly dependent as γ_1 except that γ_4 was not an inverse function of λ.

The mass flow ratio, γ_5, representing the continuation of the flow of blood to the body from the aortic arch was found to be independent of the unsteadiness parameter at least in the range $10 \leq \alpha \leq 20$ for a given Re. Within the experimental accuracy observed the dependence of γ_5 on λ could not be evaluated.

A visualization technique revealed the existence of four interdependent regions of separation for both steady and forward pulsatile flow. The formation of vortices was observed in the separated region of the main branch and double helicoidal flow was observed in branches four and five of the artificial aorta.

ACKNOWLEDGEMENTS

The author wishes to thank the following for their contributions:

- Dr. C.M. Rodkiewicz for supervising the thesis.
- Dr. N.R. Kuchar of the General Electric Space Sciences Laboratory in Philadelphia who suggested the problem to Dr. Rodkiewicz.
- Dr. G. Kubac, Specialist in Internal Medicine at the University of Alberta for his helpful suggestions.
- Dr. K. Kocandrle, Resident in Roentgenology at the University of Alberta for his assistance in the interpretation of the X-ray pictures.
- Dr. R.D. Laurenson of the Department of Anatomy, University of Alberta for his helpful suggestions.
- Mr. Golls, Technical Assistant, Department of Mechanical Engineering of the University of Alberta for his assistance with the construction of the artificial aorta.
- Mr. Jan Pospisilik, M.Sc. for help to setting the levels of constant head tanks.
- Mr. R.H. Nyren, M.Sc., for his spelling corrections.
- Mrs. M. Sherban for typing the thesis.
- My wife, Magdalena, my children Branislav and Dana for their patience.

TABLE OF CONTENTS

		Page
Abstract		iv
Acknowledgements		vi
Table of Contents		vii
List of Tables		x
List of Figures		xi
List of Symbols		xiv
CHAPTER I	INTRODUCTION	
	1.1 Introductory Remarks	1
	1.2 The General Description of the Aorta and It's Function in the Blood Circulatory System	1
	1.3 The Cardiovascular System	4
	1.4 Literature Survey	6
	1.5 Objectives of the Thesis	9
CHAPTER II	THE MATHEMATICAL MODEL	
	2.1 Introductory Remarks	10
	2.2 Derivation of Parameters	10
	2.3 Analysis of Governing Equations in Region 2	13
	2.3.1 The Continuity Equation	13
	2.3.2 The Momentum Equations	15
CHAPTER III	THE EXPERIMENTAL MODEL	
	3.1 The Range of Study	20

TABLE OF CONTENTS (continued)

		Page
3.2	Description of the Apparatus	26
3.2.1	Overall Description of the Apparatus	26
3.2.2	The Flow Unit	30
3.2.3	The Flow Rate Measurement Unit . . .	32
3.2.4	Test Section	32
3.3	The Experimental Fluid	35
3.4	Description of the Development of the Artificial Aorta	35
3.5	Flow Visualization	40
CHAPTER IV	EXPERIMENTS, RESULTS AND DISCUSSION	
4.1	Experimental Procedure	45
4.1.1	Preliminary Procedure	45
4.1.2	Actual Experimental Procedure	45
4.2	Photographic Procedure	46
4.3	Experimental Results	47
4.3.1	Steady Flow	47
4.3.2	Mass Flow Ratios as a Function of the Unsteadiness Parameter and the Reynolds Number	49
4.3.3	Mass Flow Ratios as a Function of the Reynolds Number and Unsteadiness Parameter	49

TABLE OF CONTENTS (continued)

Page

4.3.4 The Mass Flow Ratios as a Function of the Reynolds Number and the Normalized Fluctuating Component of Velocity 53

4.3.5 Description of the Flow 53

4.4 Observations and Discussions 65

4.4.1 Mass Flow Ratio 65

4.4.2 Separation Regions 76

4.5 Limitation of the Apparatus 78

CHAPTER V CONCLUSIONS

5.1 Summary 79

5.2 Suggestions for Further Work 80

REFERENCES 82

APPENDIX A SPECIFIC GRAVITY AND VISCOSITY OF THE BLOOD ANALOGUE 86

APPENDIX B PISTON STROKE CALCULATIONS 87

APPENDIX C TABLES 91

APPENDIX D ROTAMETER CALIBRATION 101

LIST OF TABLES

Table		Page
C-4.a	Dependence of Mass Flow Ratios on Re for Steady Flow of Mixture (glycerine + water) at a Static Pressure of 115 mm Hg	91
C-4.1	Dependence of Mass Flow Ratios on α for Re = 1300 and λ = 1.5	92
C-4.2	Dependence of Mass Flow Ratios on α for Re = 800 and λ = 1	93
C-4.3	Dependence of Mass Flow Ratios on α for Re = 1300 and λ = 1	94
C-4.4	Dependence of Mass Flow Ratios on α for Re = 1800 and λ = 1	95
C-4.5	Dependence of Mass Flow Ratios on Re for α = 10 and λ = 1	96
C-4.6	Dependence of Mass Flow Ratios on Re for α = 10 and λ = 1.5	97
C-4.7	Dependence of Mass Flow Ratios on Re for α = 10 and λ = 2	98
C-4.8	Dependence of Mass Flow Ratios on Re for α = 15 and λ = 2	99
C-4.9	Dependence of Mass Flow Ratios on Re for α = 19 and λ = 2	100

LIST OF FIGURES

Figure		Page
1.1	Photograph of an X-Ray Showing a Aortic Arch	3
1.2	Photograph of an X-Ray Showing the Division of Arteries Into Capillaries	3
1.3	Scheme of the Human Cardiovascular System	5
2.1	The Composition of Two Distinct Regions of the Aortic Arch	12
2.2	The Coordinate System Employed to Study flow in Region 2	12
3.1	Schematic Graph Showing: Broken Line, the Changes in Relative Total Cross-Sectional Area (on a Logarithmic Scale) of the Vascular Bed; Solid Line, the Mean Velocity in the Different Categories of Vessel, by A.C. Burton[23]	22
3.2	The Nomogram for Determining Aortic Diameter (Aortic Arch) and Aortic Biological Age in 2-m Chest X-Rays, by PD Dr. E. Strehler et al[26]	23
3.3	The Approximation of the Sinusoidal Flow in the Experimental Model	24
3.4	Apparatus Layout	27
3.5	Total View of Apparatus	28
3.6	Constant Head Tanks	31
3.7	Detail View of the Rotameter and Damping Tank	31

LIST OF FIGURES (continued)

Figure		Page
3.8	Photographs of the Flow Unit	33
3.9	Detail View of the Flow Unit	33
3.10	Graduation Vessels	34
3.11	Test Section	34
3.12	Dimensions of the Artificial Aorta	37
3.13	Stages in the Development of the Artificial Aorta. . .	38
3.14	Detail of Stage C (Figure 3.13)	39
3.15	Final Types of Artificial Aorta	39
3.16	Electrodes Housing	41
3.17	Generation Unit for Hydrogen Bubbles	41
3.18	Electronics for Hydrogen Bubble Generation	42
4.1	Dependency of Mass Flow Ratios on Re, Steady Flow (Mixture of Water and Glycerine)	48
4.2	Dependency of Mass Flow Ratios on α; Re = 1300, λ = 1.5	50
4.3	Dependency of Mass Flow Ratios on α; Re = 800, 1300 and 1800, λ = 1	51
4.4	Dependency of γ_1 on Re and α, λ = 2	52
4.5	Dependency of γ_2 on Re and α, λ = 2	54
4.6	Dependency of γ_3 on Re and α, λ = 2	55

LIST OF FIGURES (continued)

Figure		Page
4.7	Dependency of γ_4 on Re and α, $\lambda = 2$	56
4.8	Dependency of γ_5 on Re and α, $\lambda = 2$	57
4.9	Dependency of γ_1 on Re, $\alpha = 10$	58
4.10	Dependency of γ_2 on Re, $\alpha = 10$	59
4.11	Dependency of γ_3 on Re, $\alpha = 10$	60
4.12	Dependency of γ_4 on Re, $\alpha = 10$	61
4.13	Dependency of γ_5 on Re, $\alpha = 10$	62
4.14	Flow Pattern for Steady and Forward Flow by the Pulsatile Flow	64
4.15	Flow Pattern for Back Flow by the Pulsatile Flow	66
4.16	Steady Flow Characteristics for Various Reynolds Number	67
4.17	Steady Flow Characteristics for Various Reynolds Number	68
4.18	Steady Flow Characteristics for Various Reynolds Number	69
4.19	Steady Flow Characteristics for Various Reynolds Number	70
4.20	Development of Steady Flow	71
4.21	Development of Pulsatile Flow	72
4.22	Double-Helicoidal Flow in the Main Branch for Various Reynolds Number	73
D.1	Rotameter Calibration Characteristic	102

LIST OF SYMBOLS

English Symbols

C	constant ($8R^3\theta^2/D^3$)
D	unstressed internal diameter of main branch
E	Euler number ($\Delta P/\rho U^2$)
K	Dean number 1/2 ($Re\sqrt{R_o/R}$
K_m	Modified Dean number (KC)
l	length of piston stroke
L	approximate length of entrance region
L_e	length ratio (R_o/L)
P	static pressure
P_{ref}	characteristic pressure
ΔP	average pressure drop in entrance region
Q	total flow rate ($Q_1 + Q_2 + Q_3 + Q_4 + Q_5$)
Q_1	flow rate in branch (right subclavian)
Q_2	flow rate in branch (right carotid)
Q_3	flow rate in branch (left carotid)
Q_4	flow rate in branch (left subclavian)
Q_5	flow rate in main branch (flow rate to the body)
Q'	fluctuating component of the flow rate
r	radial space coordinate
R	radius of the curvature
Re	Reynolds number (UD/ν)
R_o	unstressed internal radius
s	length of the arch at the centreline of the tube ($R\theta$)

S	Strouhal number (L/UT_o)
t	time variable
T_o	period for one pulse
U	average longitudinal velocity at the entrance
U'	fluctuating component of velocity at the entrance
V_a	reference average velocity
z	axis in cylindrical coordinates

Greek Symbols

α	unsteadiness parameter ($D\sqrt{\omega/\nu}$)
γ_1	mass flow ratio (Q_1/Q)
γ_2	mass flow ratio (Q_2/Q)
γ_3	mass flow ratio (Q_3/Q)
γ_4	mass flow ratio (Q_4/Q)
γ_5	mass flow ratio (Q_5/Q)
θ	angle of the curvature
λ	normalized velocity fluctuation ($U'/\hat{U}$)
μ	absolute fluid viscosity
ν	kinematic fluid viscosity (μ/ρ)
ρ	fluid density
ϕ	azimuthal space in cylindrical coordinates
ω	pulse rate ($1/T_o$)

CHAPTER I

INTRODUCTION

1.1 Introductory Remarks

An important cause of death is diseases and defects of the cardiovascular system. Thus fundamental research into this system is being pursued. The flow of blood through the vessels is one of the aspects of this system well suited for engineering research. It is essentially a problem in fluid mechanics, albeit a rather complicated one.

The purpose of this thesis is to ascertain the dependance of the flow rate in the downstream branches of a certain artificial aorta on the non-dimensional parameters: Reynolds number, unsteadiness parameter and velocity fluctuation parameter. The high degree of complexity of the physical laws and equations describing blood flow necessitate that the study of this problem is experimental rather than analytical.

1.2 The General Description of the Aorta and Its Function in the Blood Circulatory System

The aorta is the great trunk artery that carries blood from the heart to be distributed by branch arteries through the body. The aorta is a wide tube with thick walls which are largely composed of elastic tissue[1]; and like any other elastic structure, its capacity is determined largely by the pressure of the blood it contains. When blood is expelled during ventricular systole, the

aortic pressure rises, the aorta is distended and so accommodates a large part of the blood expelled, the remainder escaping through the arteries. During ventricular diastole, the tension in the aortic walls maintains the flow of blood onwards through the arteries, and the aorta diminishes in size until it is again distended at the next heart beat. In this purely passive way the aorta (and to a less extent its larger branches which are similar in structure) converts the intermittent flow from the heart into a continuous though pulsating flow in the arteries. As can be seen in Figure 1.1* the blood passes from the aorta into the main branches. The arteries divide repeatedly until they become capillaries. (See Figure 1.2*). With each subdivision, the arterial lumen becomes smaller and the arterial wall becomes more predominantly muscular. By the contraction or relaxation of their muscular walls, the arteries (particularly the smaller branches or arterioles) are capable of great variation in calibre, and it is this calibre which largely determines the proportion of the total cardiac output distributed to the individual organs.

Moreover, the total cardiac output could be influenced by arterial diseases. Mitchell and Schwartz[2] state that arterial disorders are known by such names as arteriosclerosis, atheroma, and atherosclerosis. The most widely adopted term, atherosclerosis, will be used in this thesis. It will refer to the buildup of fatty and/or fibrous plagues which occlude the vessel and destroy the

---

* X-Ray pictures were taken at the University of Alberta Hospital.

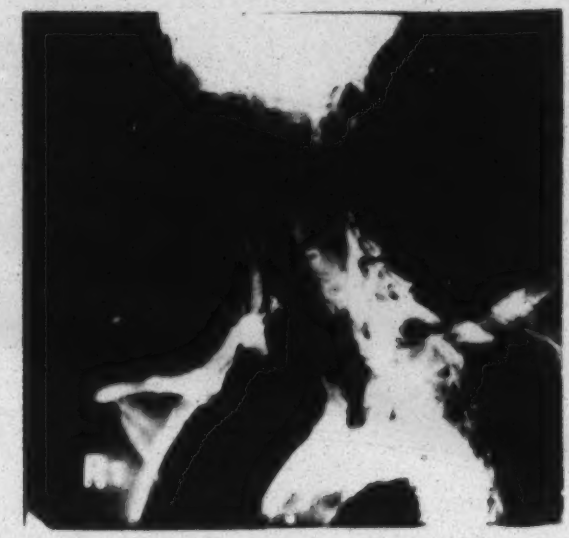

Figure 1.1 Photograph of an X - Ray Showing a Aortic Arch

Figure 1.2 Photograph of an X - Ray Showing the Division of Arteries Into Capillaries

elasticity of its walls.

1.3 The Cardiovascular System*

The human cardiovascular system consists of two pumps connected in series with two circulations as shown in Figure 1.3. The left ventricle pumps freshly oxygenated blood through the aorta into the systematic circulation which leads to arteries going to the head, internal organs and limbs. As the various organs are perfused with this oxygen-rich blood, oxygen is diffused from the blood into the cells of the organs. As the blood becomes depleted of its oxygen supply it returns to the right atrium and right ventricle by means of lesser and greater veins. The right ventricle pumps the blood through the pulmonary circulation (lungs) where oxygen from the atmosphere is diffused into the blood. The oxygenated blood then continues on to the left atrium and left ventricle by means of the pulmonary veins and the cycle thus continues.

The two ventricles work in unison, both discharging their load of blood simultaneously into their outlets or arteries. This phase of the heartbeat the expulsion of the blood by contraction of the ventricles, is called systole. The phase in which the ventricles are filled with blood, each from its own atrium, is called diastole. The left and right ventricles must pump an equal volume of blood over a period of time.

---

* This section comes before the literature survey in the hope that any unfamiliar terms used in the survey will have been explained adequately to those readers unfamiliar with a physiological terminology.

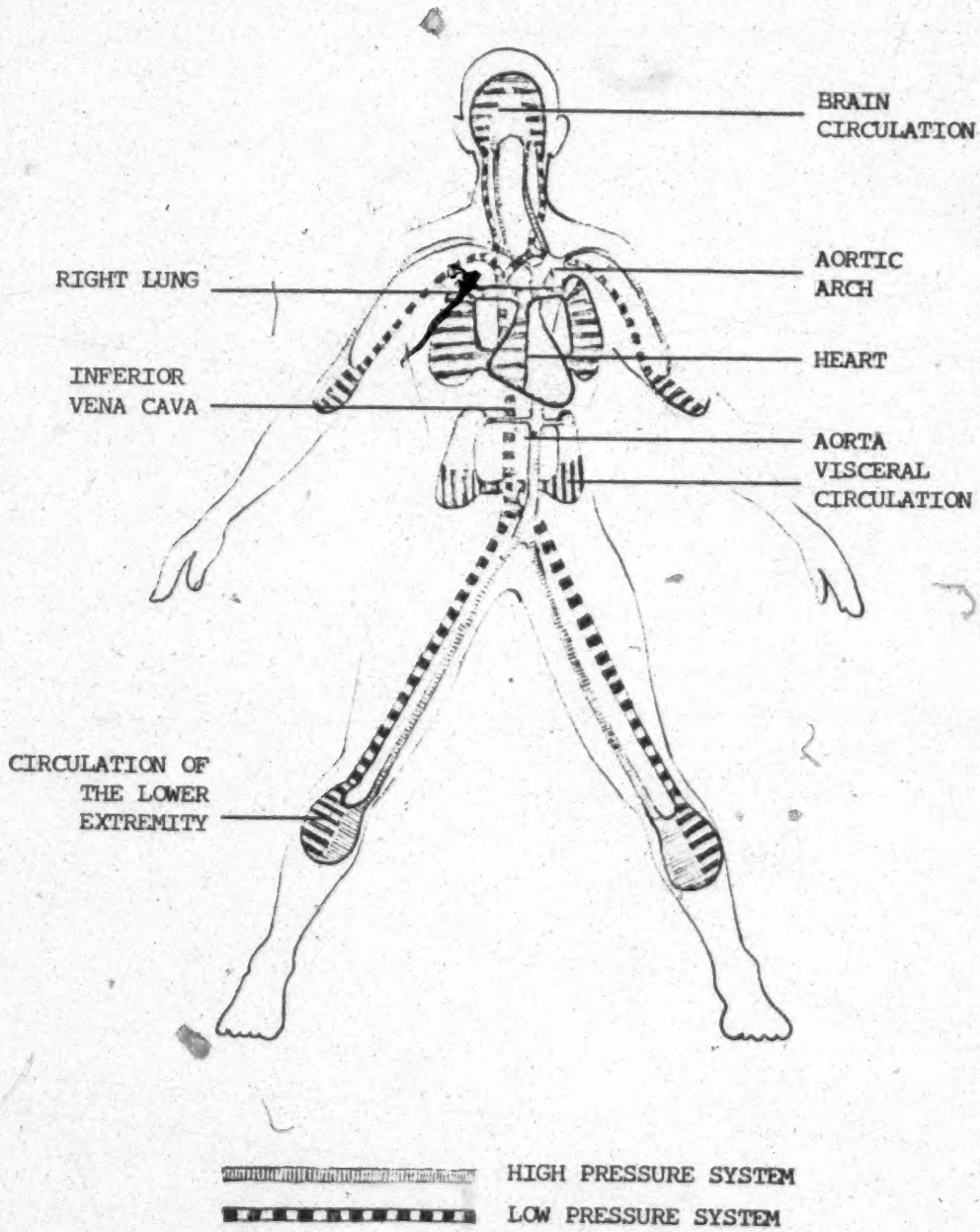

Figure 1.3: Scheme of the Human Cardiovascular System

1.4 Literature Survey

As mentioned previously the blood flow problem lies in a wide and complicated field. At the present time, the exact nature of blood flow in the human ascending aorta is not known. Particularly the elastic deformations of the vessel make a theoretical approach very difficult. Theoretical considerations as well as results obtained from model experiments by J.G. Porje[3], confirm the supposition that the effects of viscosity and elasticity are of secondary order of magnitude and that the equations valid for calculation of nonviscous flow will therefore give a reasonable approximation of the calculation of instantaneous flow in the ascending aorta. Fully developed flow can only exist in the flow field distant from the ends of the tube where end effects are negligible. Atabek[4] considered these end effects in developing an inlet length theory for periodic flow in tubes with rigid walls.

Kuchar and Ostrach[5] considered entrance effects associated with laminar flows of viscous fluids in circular elastic tubes. Of particular interest was their derivation of the significant dimensionless parameters. Chapter II of present work reviews these dimensionless parameters.

The problem becomes even more complex in the case of branched vessels and, consequently, most of the work in this area is done with the help of experimental models rather than adopting a purely theoretical approach.

G.S. Malindzak Jr.[6] discussed the derivation of a system of mathematical equations to describe the transmission and reflection of arterial pressure pulses in the mammalian circulatory system. His theoretical analysis involves calculation of incident and reflected wave parameters derived from dependence of time, space and pressure data. Specifically, the paper describes the theoretical basis for numerical analysis resulting in values for reflected energy, phase velocities in the aorta, as well as experiments in which such analysis has been applied in the anesthetized dog.

Robert H. Cox[7] reviewed the linearized wave propagation model which can be used to predict both transmission characteristics and hydraulic fluid impedance values upon system input parameters. Most of the models considered the propagation of small, axisymmetric, harmonic disturbances through an incompressible, Newtonian fluid contained within a distensible tube of long length.

J.W. Amyot et al[8] measured the sequential velocity development in the ascending aorta using a conical hot-film probe in six anesthetized dogs. Sequential velocity developments during systole are presented and instantaneous volumetric flows are obtained from the integrated profiles. The calculated flows are in agreement with standard measurements of cardiac output. The measurements show that maximum reverse flow occurs at the end systole when the dicrotic notch is observed in aortic pressure trace. Nonsymmetry was observed in the sequential velocity profiles during the early phases of ejection, followed by more nearly symmetric profiles as the flow decelerated.

Donald L. Fry et al[9] derived a method of determining the instantaneous aortic blood velocity from the Navier-Stokes equation. Experimental support for the derived formulae was obtained in a flow model and in a living animal aorta.

Marrill P. Spencer and A.B. Denison[10] presented the exact blood flow curves of the aorta and established their validity by their relationship to the differential pressures existing along that structure. They pointed out some artifacts that may be introduced into flow curves when recorded under certain conditions which considerably alter the normal physical characteristics of the arterial system.

M.F. Snyder et al[11] devised a model of the human systematic arterial tree based on a lumped-parameter-circuit approximate form. This model has been set up and studied on an analog computer. A feature of this simulation is the division of the arterial system into sections whose lengths are inversely proportional (approximately) to their cross-sectional area - or what they termed "equal-volume" modeling. The simulated pressure and flow waveforms obtained with the model compare favourably with data recorded from the normal adult human, and exhibit such well-known features as distal delay and peaking of pressure pulses. The predicted aortic input impedance dependency on frequency checks well against measurements on the human. The model also provides a simple means for determination of cardiac output, cardiac work and cardiac power under various assumed conditions such as variation of heart rate.

1.5 Objectives of the Thesis

The most sophisticated blood flow in arteries seems to be within the aorta. It is the purpose of this thesis to study the flow through the main branches of one such bifurcation and to find out what influences the mass flow ratios γ_1, γ_2, γ_3, γ_4 and γ_5 throughout the artificial aorta, particularly when the significant dimensionless parameters are varied.

In addition to the dimensionless numbers used by Rodkiewicz and Howell[12], it was decided to incorporate the characteristic values introduced by Ito[13]. Furthermore a modified Dean number Km (product of the Dean number and a constant) will be introduced.

Some qualitative observations of flow characteristics in a bifurcation will be made using the visualization technique used by Rodkiewicz and Roussel[14].

CHAPTER II

THE MATHEMATICAL MODEL

2.1 Introductory Remarks

The solution of the mathematical model to encompass and completely describe the physical processes occurring throughout the blood circulation system is not possible at the present time. The mathematical model is described in the next section, and is subject to the following assumptions.

1. Blood is considered to be a homogeneous incompressible Newtonian fluid with a constant viscosity.
2. The vessel will be considered to be circular.
3. The tube walls of the bifurcation will not be flexible.
4. The tube will be considered to be externally constrained in such a manner that no longitudinal displacement or motion of the bifurcation wall occurs.
5. This model applies to the macrocirculation (large arteries and veins), but not to the microcirculation (arteries, capillaries, and venules).

2.2 Derivation of Parameters

The purpose of the mathematical models as far as this thesis is concerned is to allow the derivation of the significant parameters. The problem under study may be thought to be composed of two classical cases of the flow, through the straight pipe and flow through curved pipe. The two distinct regions are shown in Figure 2.1.

Kuchar and Ostrach[5] and Kuchar and Scala[15] developed the following non-dimensional parameters for pulsating flow in region 1.

$$\text{Reynolds' Number, } Re = \frac{UR_o}{\nu}$$

$$\text{Strouhal Number, } S = \frac{L}{UT_o}$$

$$\text{Length Ratio, } L_e = \frac{R_o}{L}$$

$$\text{Euler Number, } E = \frac{\Delta P}{\rho U^2}$$

The unsteadiness parameter, α, developed by Kuchar and Scala[15] is as follows:

$$\alpha = \sqrt{Re \times S \times L_e} = \sqrt{\frac{UR_o}{\nu} \times \frac{L}{UT_o} \times \frac{R_o}{L}}$$

$$= R_o\sqrt{\frac{1}{\nu T_o}} \qquad (2.2)$$

If the pulse rate is defined as $\omega = \frac{1}{T_o}$, equations (2.2) become

$$\alpha = R_o\sqrt{\frac{\omega}{\nu}}$$

Two pertinent dimensionless parameters to be considered are:

$$R_e = \frac{UD}{\nu} \qquad (2.3)$$

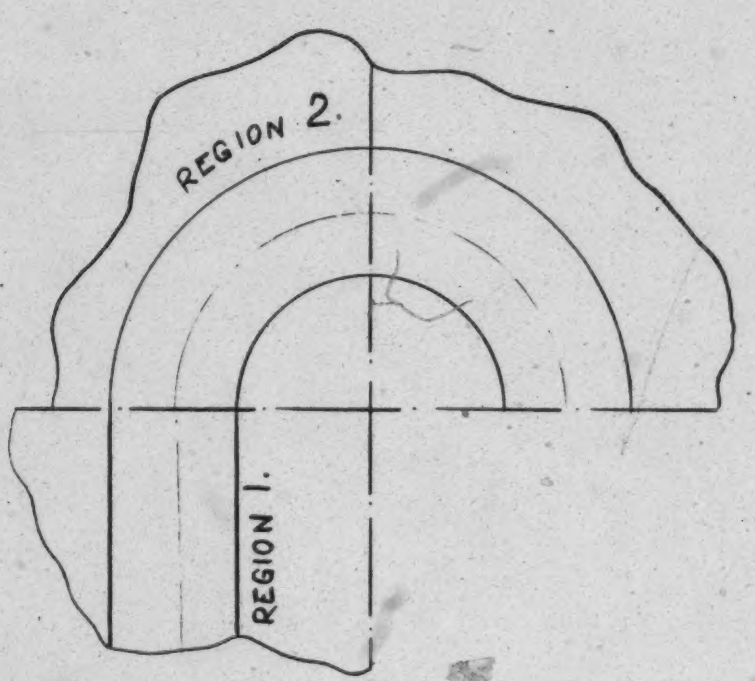

Figure 2.1: The Composition of Two Distinct Regions of the Aortic Arch

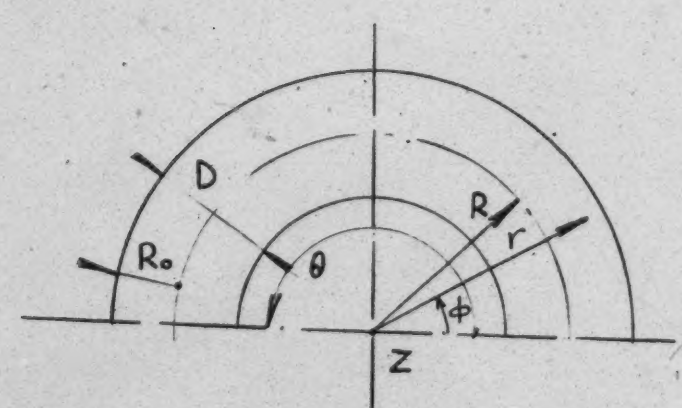

Figure 2.2: The Coordinate System Employed to Study Flow in Region 2

$$\alpha = D\sqrt{\frac{\omega}{\nu}} \qquad (2.4)$$

In this region, it should be noted that Re is calculated at the entrance to the bifurcation.

Rodkiewicz and Howell[12] considered three parameters, Re, α, and λ where α, in equation (2.4), is a modified form of the unsteadiness parameter used by Kuchar and Scala[15].

Region 2, which is composed of the main arch (upper and lower aortic arch) of the artificial aorta, is considered to have a constant cross-section. Examination of several x-rays showed that though a change in diameter along the arch length does exist this deviation was neglected.

The preceding considerations concerning pipe flow are valid only for straight pipes. In curved pipes there exists a secondary flow[16,17] because the particles near the flow axis which have higher velocity are acted upon by a larger centrifugal force than the slower particles near the walls. This leads to the emergence of a secondary flow which is directed outwards in the centre and inwards (i.e. towards the centre of curvature) near the wall.

The characteristic dimensionless variable, which determines the influence of curvature in the laminar case, is the Dean Number[18,19], K.

$$K = \frac{1}{2} Re\sqrt{\frac{R_o}{R}} \qquad (2.5)$$

The coordinate system employed to study region 2 is shown in Figure 2.2. The z axis is perpendicular to the plane of the page.

2.3 Analysis of Governing Equations in Region 2

2.3.1 The Continuity Equation

The continuity equation for cylindrical coordinates is given by

$$\frac{1}{r}\frac{\partial}{\partial r}(\rho r V_r) + \frac{1}{r}\frac{\partial}{\partial \phi}(\rho V_\phi) + \frac{\partial}{\partial_z}(\rho V_z) = 0 \qquad (2.6)$$

Defining the arch length of the tube centerline as

$$s = R\theta \qquad (2.7)$$

and introducing the following characteristic values used by H. Ito[13]:

$$\bar{V}_r = \frac{V_r s}{\nu}, \quad \bar{z} = \frac{z}{s}, \quad V_a = Q/\text{area}$$

$$\bar{V}_\phi = \frac{V_\phi}{V_a}, \quad \bar{r} = \frac{r}{s}, \qquad (2.8)$$

$$\bar{V}_z = \frac{V_z s}{\nu}, \quad \bar{\phi} = \frac{\phi}{\theta},$$

where, V_a is average velocity, and $\bar{\phi}$ is in range $0 \leq \bar{\phi} \leq 1$; substituting into the continuity equation (2.6), assuming ρ to be constant, the equation is reduced to the following non-dimensional form

$$\frac{1}{\bar{r}}\frac{\partial}{\partial \bar{r}}(\bar{r}\bar{V}_r) + \left[\frac{V_a s}{\nu\theta}\right]\frac{1}{\bar{r}}\frac{\partial}{\partial \bar{\phi}}(\bar{V}_\phi) + \frac{\partial}{\partial \bar{z}}(\bar{V}_z) = 0$$

Consider the non-dimensional parameter $\frac{V_a s}{\nu\theta}$, the leading coefficient of the second term of the above equation. Since $s = R\theta$ and $R = R_o R/R_o$ this parameter can be expressed as

$$\frac{V_a}{\nu\theta} = \frac{V_a R}{\nu} = \frac{V_a R_o}{\nu}\frac{R}{R_o} \tag{2.9}$$

Therefore, the continuity equation can be rewritten as

$$\frac{1}{\bar{r}}\frac{\partial}{\partial \bar{r}}(\bar{r}\,\bar{V}_r) + \left[\frac{V_a R_o}{\nu}\right]\left[\frac{R}{R_o}\right]\frac{1}{\bar{r}}\frac{\partial}{\partial \bar{\phi}}(\bar{V}_\phi) + \frac{\partial}{\partial \bar{z}}(\bar{V}_z) = 0 \tag{2.10}$$

2.3.2 The Momentum Equations

The momentum equations governing steady flow in cylindrical coordinates are given by

$$V_r\frac{\partial V_r}{\partial r} + \frac{V_\phi}{r}\frac{\partial V_r}{\partial \phi} - \frac{V_\phi^2}{r} + \bar{V}_z\frac{\partial V_r}{\partial z} = -\frac{1}{\rho}\frac{\partial P}{\partial r} + g_r +$$

$$+ \nu\left\{\frac{\partial^2 V_r}{\partial r^2} + \frac{1}{r}\frac{\partial V_r}{\partial r} - \frac{Vr}{r^2} + \frac{1}{r^2}\frac{\partial^2 V_r}{\partial \phi^2} - \frac{2}{r^2}\frac{\partial V_\phi}{\partial \phi} + \frac{\partial^2 V_r}{\partial z^2}\right\} \tag{2.11}$$

$$V_r\frac{\partial z}{\partial r} + \frac{V_\phi}{r}\frac{\partial V_z}{\partial \phi} + V_z\frac{\partial V_z}{\partial z} = -\frac{1}{\rho}\frac{\partial P}{\partial z} + g_z +$$

$$+ \nu\left\{\frac{\partial^2 V_z}{\partial r^2} + \frac{1}{r}\frac{\partial V_z}{\partial r} + \frac{1}{r^2}\frac{\partial^2 V_z}{\partial \phi^2} + \frac{\partial^2 V_z}{\partial z^2}\right\}$$

$$V_r\frac{\partial \phi}{\partial r} + \frac{V_\phi}{r}\frac{\partial V_\phi}{\partial \phi} + \frac{V_r V_\phi}{r} + V_z\frac{\partial V_\phi}{\partial z} = -\frac{1}{\rho}\frac{\partial P}{\partial \phi} + g_\phi +$$

$$+ \nu\left\{\frac{\partial^2 V_\phi}{\partial r^2} + \frac{1}{r}\frac{\partial V_\phi}{\partial r} - \frac{V_\phi}{r^2} + \frac{1}{r^2}\frac{\partial^2 V_\phi}{\partial \phi^2} + \frac{2}{r^2}\frac{\partial V_r}{\partial \phi} + \frac{\partial^2 V_\phi}{\partial z^2}\right\}$$

Let $\bar{P} = P/P_{ref}$, where P_{ref} = characteristic pressure, to be determined later.

Substituting (2.7) and (2.8) into momentum equations (2.11), and dividing the first and the second by ν^2/s^3, and the third equation by $V_a\,\nu/s^2$, the equations are reduced to the following non-dimensional forms.

$$\bar{V}_r \frac{\partial \bar{V}_r}{\partial \bar{r}} + \frac{\bar{V}_\phi}{\bar{r}} \frac{\partial \bar{V}_r}{\partial \phi} - \left[\frac{V_a^2 s^2}{\nu^2}\right] \frac{\bar{V}_\phi^2}{\bar{r}} + \bar{V}_z \frac{\partial \bar{V}_r}{\partial \bar{z}} = - \left[\frac{P_{ref} s^2}{\rho \nu^2}\right] \frac{\partial \bar{P}}{\partial \bar{r}} + \left[\frac{s^3}{\nu^2}\right] g_r +$$

$$+ \frac{\partial^2 \bar{V}_r}{\partial \bar{r}^2} + \frac{1}{\bar{r}} \frac{\partial \bar{V}_r}{\partial \bar{r}} - \frac{\bar{V}_r}{\bar{r}^2} + \left[\frac{\nu^2}{s^2 V_a^2}\right] \frac{1}{\bar{r}^2} \frac{\partial^2 \bar{V}_r}{\partial \phi^2} - \frac{2}{\bar{r}^2} \frac{\partial \bar{V}_\phi}{\partial \phi} + \frac{\partial^2 \bar{V}_r}{\partial \bar{z}^2} ;$$

$$\bar{V}_r \frac{\partial \bar{V}_z}{\partial \bar{r}} + \frac{\bar{V}_\phi}{\bar{r}} \frac{\partial \bar{V}_z}{\partial \phi} + \bar{V}_z \frac{\partial \bar{V}_z}{\partial \bar{z}} = - \left[\frac{P_{ref} s^2}{\rho \nu^2}\right] \frac{\partial \bar{P}}{\partial \bar{z}} + \left[\frac{s^3}{\nu^2}\right] g_r + \frac{\partial^2 \bar{V}_z}{\partial \bar{r}^2} +$$

$$+ \frac{1}{\bar{r}} \frac{\partial \bar{V}_z}{\partial \bar{r}} + \left[\frac{\nu^2}{s^2 V_a^2}\right] \frac{1}{\bar{r}^2} \frac{\partial^2 \bar{V}_z}{\partial \phi^2} + \frac{\partial^2 \bar{V}_z}{\partial \bar{z}^2} \qquad (2.12)$$

$$\bar{V}_r \frac{\partial \bar{V}_\phi}{\partial \bar{r}} + \frac{\bar{V}_\phi}{\bar{r}} \frac{\partial \bar{V}_\phi}{\partial \phi} + \frac{\bar{V}_r \bar{V}_\phi}{\bar{r}} + \bar{V}_z \frac{\partial \bar{V}_\phi}{\partial \bar{z}} = - \left[\frac{1}{\rho} \frac{P_{ref}}{V_a^2}\right] \frac{1}{\bar{r}} \frac{\partial \bar{P}}{\partial \phi} +$$

$$+ \left[\frac{s^2}{V_a \nu}\right] g_\phi + \frac{\partial^2 \bar{V}_\phi}{\partial \bar{r}^2} + \frac{1}{\bar{r}} \frac{\partial \bar{V}_\phi}{\partial \bar{r}} - \frac{\bar{V}_\phi}{\bar{r}^2} + \left[\frac{\nu^2}{s^2 V_a^2}\right] \frac{1}{\bar{r}^2} \frac{\partial^2 \bar{V}_\phi}{\partial \phi^2} +$$

$$+ \left[\frac{\nu^2}{s^2 V_a^2}\right] \frac{2}{\bar{r}^2} \frac{\partial \bar{V}_r}{\partial \phi} + \frac{\partial^2 \bar{V}_\phi}{\partial \bar{z}^2}$$

Consider the dimensionless groupings of equations (2.12).

Defining

$$K_m^2 = V_a^2 \, s^2/\nu^2$$

which can be written as

$$\frac{1}{4} K_m^2 = \frac{1}{4} \left[Re^2 \frac{D/2}{R}\right]\left[\frac{s^2}{D^2} \frac{R}{D/2}\right] \tag{2.13}$$

and since the Dean Number is defined as $K = \frac{1}{2} Re \sqrt{\frac{R_o}{R}}$

from which

$$K^2 = \frac{1}{4} Re^2 \frac{R_o}{R} \tag{2.14}$$

Combining equations 2.14 and 2.13 using equation 2.7 gives

$$K_m^2 = K^2 C$$

where

$$C = \frac{8R^3\theta^2}{D^3} \tag{2.15}$$

Since the radial pressure gradient term cannot be neglected, choose

$$P_{ref} = \frac{\rho\nu^2}{s^2} \tag{2.16}$$

so that

$$\left[\frac{P_{ref}\, s^2}{\rho \nu^2}\right] = 1 \tag{2.17}$$

Let

$$f_r = \left[\frac{\nu^2}{s^3}\right], \tag{2.18}$$

then body forces in the radial momentum equation are very small when $f_r \gg 1$.

Let

$$f_\phi = \frac{V_a\, \nu}{2}, \tag{2.19}$$

then body forces in the azimuthal momentum equation are very small when $f_\phi \gg 1$, i.e. V_a is very large and/or s is very small.

Equations (2.16) and (2.13) show that

$$\left[\frac{1}{\rho}\frac{P_{ref}}{V_a^2}\right] = \frac{1}{K_m^2} \tag{2.20}$$

Thus the final form of the non-dimensionalized momentum equations is

$$\bar{V}_r \frac{\partial \bar{V}_r}{\partial \bar{r}} + \frac{\bar{V}_\phi}{\bar{r}} \frac{\partial \bar{V}_r}{\partial \bar{\phi}} - [K_m^2] \frac{\bar{V}_\phi^2}{\bar{r}} + \bar{V}_z \frac{\partial \bar{V}_r}{\partial \bar{z}} = - \frac{\partial \bar{P}}{\partial \bar{r}} + \left[\frac{1}{f_r}\right] g_r + \frac{\partial^2 \bar{V}_r}{\partial \bar{r}^2} +$$

$$+ \frac{\partial \bar{V}_r}{\partial \bar{r}} \frac{1}{\bar{r}} + \frac{\bar{V}_r}{\bar{r}^2} + \left[\frac{1}{K_m^2}\right] \frac{1}{\bar{r}^2} \frac{\partial^2 \bar{V}_r}{\partial \bar{\phi}^2} - \frac{2}{\bar{r}^2} \frac{\partial \bar{V}_\phi}{\partial \bar{\phi}} + \frac{\partial^2 \bar{V}_r}{\partial \bar{z}^2} \quad , \tag{2.21a}$$

$$\bar{V}_r \frac{\partial \bar{V}_z}{\partial \bar{r}} + \frac{\bar{V}_\phi}{\bar{r}} \frac{\partial \bar{V}_z}{\partial \bar{\phi}} + \bar{V}_z \frac{\partial \bar{V}_z}{\partial \bar{z}} = - \frac{\partial \bar{P}}{\partial \bar{z}} + \left[\frac{1}{f_z}\right] g_z +$$

$$+ \frac{\partial^2 \bar{V}_z}{\partial \bar{r}^2} + \frac{1}{\bar{r}} \frac{\partial \bar{V}_z}{\partial \bar{r}} + \left[\frac{1}{K_m^2}\right] \frac{1}{\bar{r}^2} \frac{\partial^2 \bar{V}_z}{\partial \bar{\phi}^2} + \frac{\partial^2 \bar{V}_z}{\partial \bar{z}^2} \quad , \tag{2.21b}$$

$$\bar{V}_r \frac{\partial \bar{V}_\phi}{\partial \bar{r}} + \frac{\bar{V}_\phi}{\bar{r}} \frac{\partial \bar{V}_\phi}{\partial \bar{\phi}} + \frac{\bar{V}_r \bar{V}_\phi}{\bar{r}} + \bar{V}_z \frac{\partial \bar{V}_\phi}{\partial \bar{z}} = - \left[\frac{1}{K_m^2}\right] \frac{1}{\bar{r}} \frac{\partial \bar{P}}{\partial \bar{\phi}} +$$

$$+ \left[\frac{1}{f_\phi}\right] g_\phi + \frac{\partial^2 \bar{V}_\phi}{\partial \bar{r}^2} + \frac{1}{\bar{r}} \frac{\partial \bar{V}_\phi}{\partial \bar{r}} - \frac{\bar{V}_\phi}{\bar{r}^2} + \left[\frac{1}{K_m^2}\right] \frac{1}{\bar{r}^2} \frac{\partial^2 \bar{V}_\phi}{\partial \bar{\phi}^2} +$$

$$+ \left[\frac{1}{K_m^2}\right] \frac{2}{\bar{r}^2} \frac{\partial \bar{V}_r}{\partial \bar{\phi}} + \frac{\partial^2 \bar{V}_\phi}{\partial \bar{z}^2} \quad . \tag{2.21c}$$

CHAPTER III

THE EXPERIMENTAL MODEL

The arterial system is, at its simplest, a system of conduits carrying fluid from a source pump to the capillaries. That this system defies elegant and accurate analysis can be attributed largely to the fact that the pump never delivers a stroke which is exactly the same as any other stroke; no two aortas have exactly the same dimensions and mechanical properties; no system of branches ever exactly duplicates any other system of branches; all of the tubes are tapering and are made of materials which exhibit non-linear behaviour, and they are filled with fluid which is non-homogeneous and anomalous in behaviour.

3.1 The Range of Study

The expressions for the Reynolds number and unsteadiness parameter as described by equations (2.3) and (2.4) have been developed. It is now necessary to determine the range of these parameters for the physiological case. To do this, the following data has been gleaned from Wintrobe[20], Tuttle and Schottelius[21], and Bell, Davidson, and Scarborough[22]:

1. Blood density varies from 1.048 to 1.066 gm/cm^3.
2. The relative viscosity of blood with respect to distilled water varies from 3.5 to 5.4.
3. The kinematic viscosity of distilled water equals 0.010027 cm^2/sec.

4. Referring to Figure 3.1, for the case in study where $2.1 \leq D \leq 3$, the minimum velocity is approximately 13 cm/sec and the maximum is 20 cm/sec.
5. Using the Nomogram (Figure 3.2) for Determining Normal Aortic Diameter (Aortic Arch) from P.D. Dr. E. Strehler[26] the diameter is found to vary from 2.1 cm up to a maximum of 3 cm.
6. Human pulse rate varies from 50 to 100 beats per minute.

Substitution of this data into equations (2.3) and (2.4) yields the following ranges of study:

$$528 \leq Re \leq 1823 \tag{3.1}$$

$$9.47 \leq \alpha \leq 19.14 \tag{3.2}$$

The flow from the heart will be approximated as a sinusoidal type flow as illustrated in Figure 3.3.

The normalized velocity fluctuation is defined by the following expression:

$$\lambda = \frac{U'}{U} \tag{3.3}$$

where U is mean velocity and U' is the fluctuating component of velocity. Kuchar and Scala[15] report the physiological range for λ to be as follows:

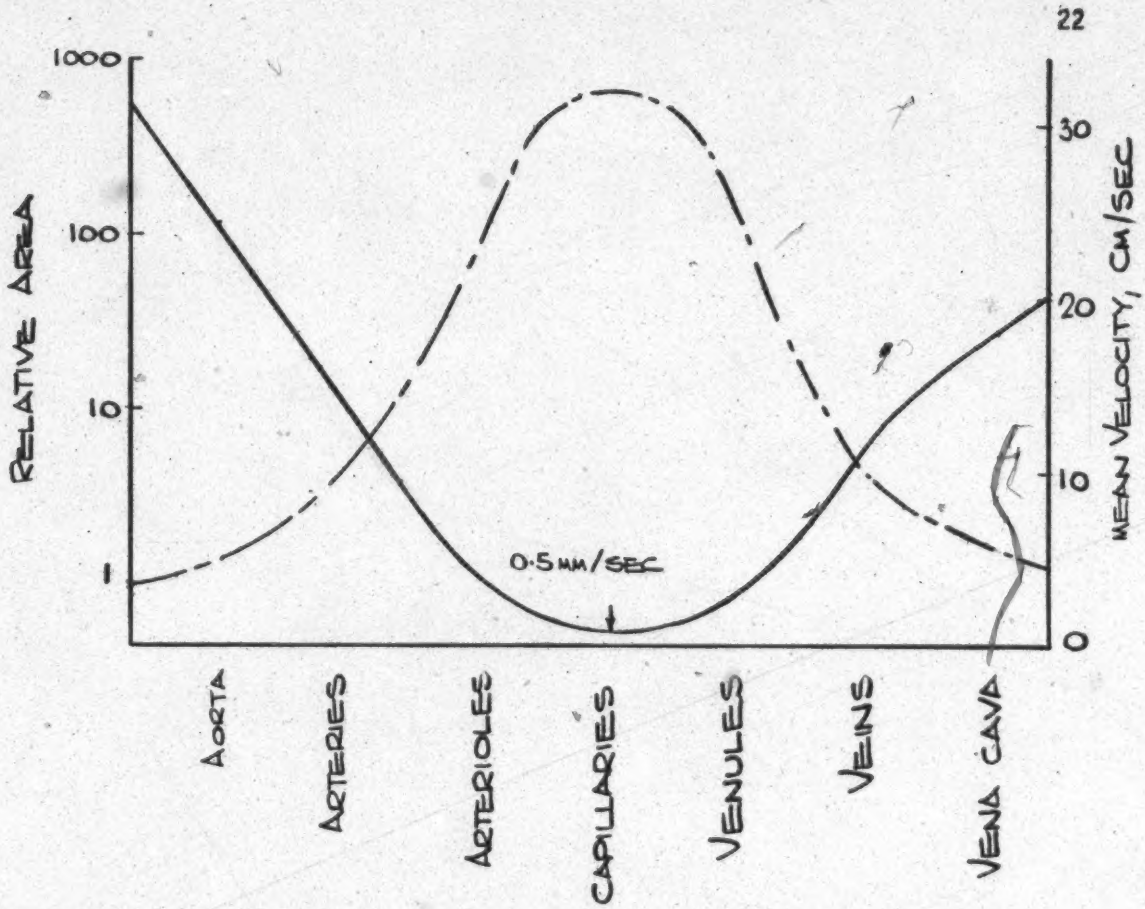

Figure 3.1: Schematic Graph Showing: Broken Line, the Changes in Relative Total Cross-Sectional Area (on a Logarithmic Scale) of the Vascular Bed; Solid Line, the Mean Velocity in the Different Categories of Vessel, by A.C. Burton[23]

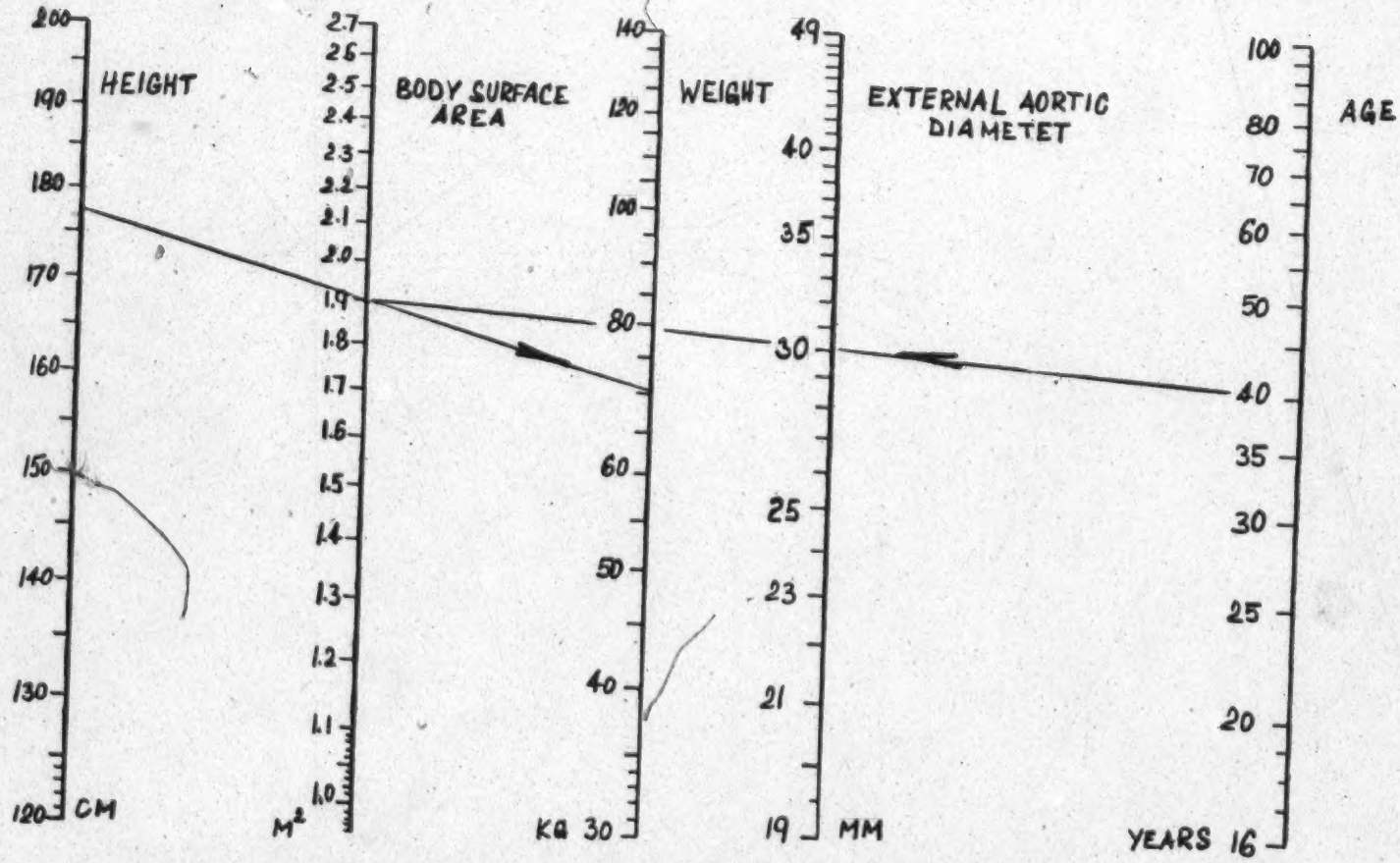

Figure 3.2: The Nomogram for Determining Aortic Diameter (Aortic Arch) and Aortic Biological Age in 2-m Chest X-Rays, by PD Dr. E. Strehler et al[26]

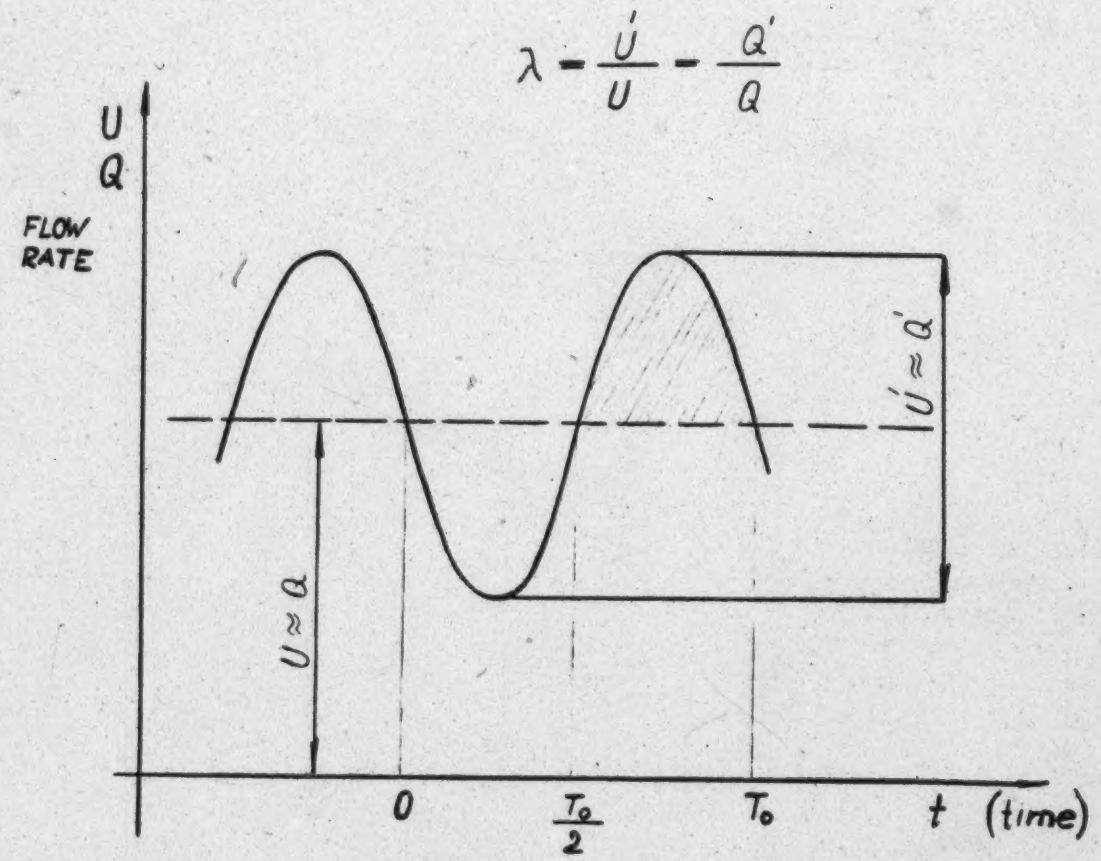

Figure 3.3: The Approximation of the Sinusoidal Flow in the Experimental Model

$$1 < \lambda < 2 \tag{3.4}$$

Weiting[24] found that a 36.7% glycerol-aqueous solution was a good hydraulic analogue for blood. The specific gravity of this mixture is 1.10 and the viscosity is 4.5 centipoise. Calculations of these quantities are in Appendix A. This viscosity falls within the range accepted for human blood (3.5 to 5.4 cp.) and the specific gravity is reasonably close (1.048 to 1.066).

Substituting the kinematic viscosity of the blood analogue ($\nu = 0.045/1.1$) and the main branch diameter ($D = 2.8$ cm. = 1.113") of the experimental model into the relationships for Re and α yields the following relationships:

$$Re = 185.2 \times Q \tag{3.5}$$

$$\alpha = 1.785 \sqrt{\omega} \tag{3.6}$$

Where ω is measured in cycles per minute and Q is measured in liters/min.

Substituting equations (3.5) and (3.6) into (3.1) and (3.2) yields the ranges of flow rate and pulse rate the experimental model must be capable of:

$$2.85 < Q < 9.84 \tag{3.7}$$

$$28 < \omega < 115 \tag{3.8}$$

In the experiments the required range of the normalized velocity fluctuation, λ, was covered by the use of different sized cams. In Appendix B the interdependence of the length of the piston stroke, l, the velocity fluctuation, λ, the flow rate, Q, and the pulse rate, ω, is outlined. The relationship is:

$$l = 0.770\ \lambda Q/\omega \qquad (3.9)$$

where l is measured in inches.

3.2 Description of the Apparatus

3.2.1 Overall Description of the Apparatus

Figures 3.4 and 3.5 show the layout and a photograph of the apparatus, respectively. The apparatus can be divided into three sections:

1. The flow unit,
2. The flow rate measurement unit,
3. The test section.

Sections (2) and (3) were placed on a table. The test section was connected to the flow unit by copper pipes and flexible tubings of 1.25 inch internal diameter.

The inlet and outlet connections of the bifurcation were made of surgical tubing.* The upstream branch was approximately

---

* "Jayon" Surgical Tubing Johnston Industrial Plastics, Edmonton, Alberta.

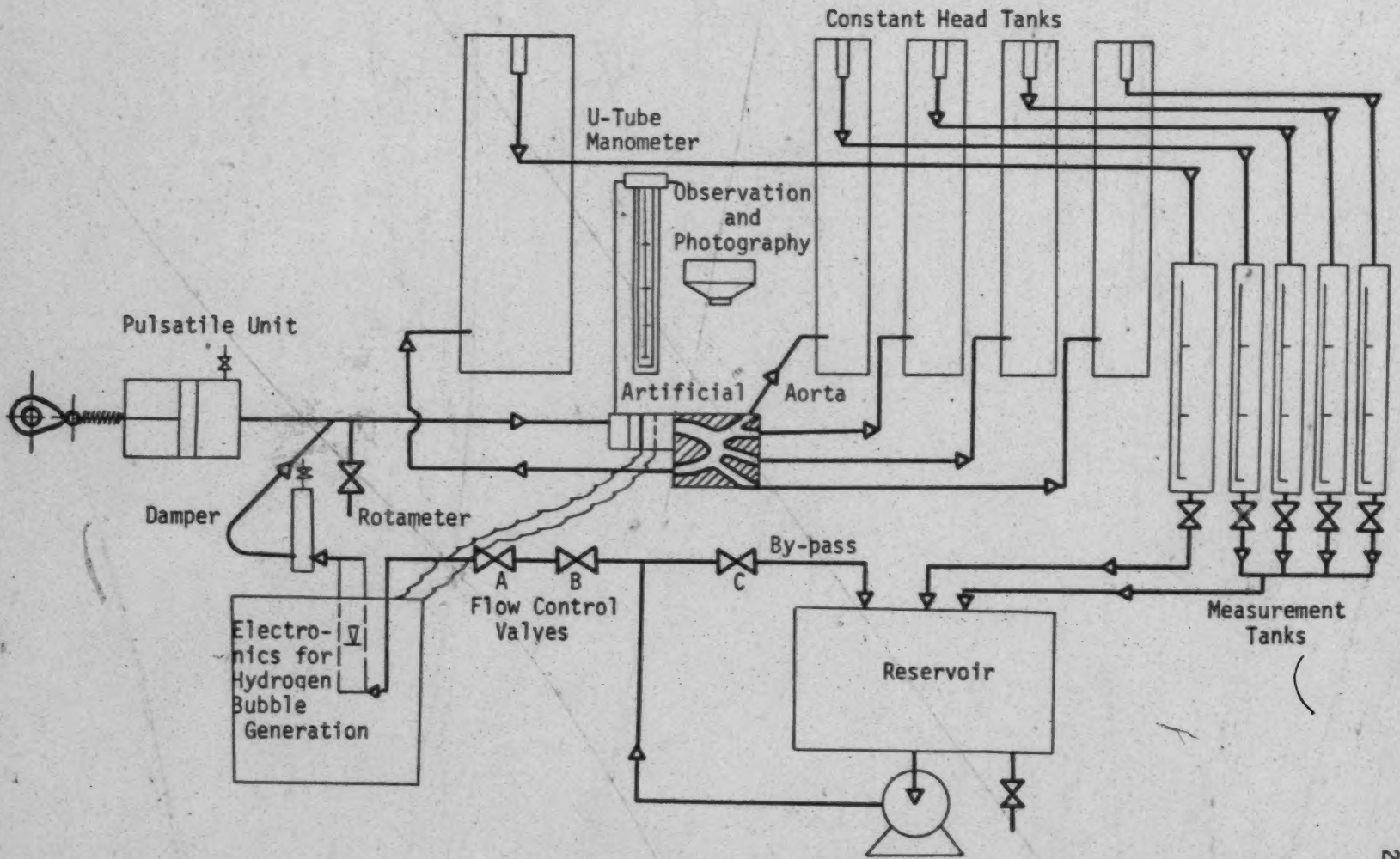

Figure 3.4: Apparatus Layout

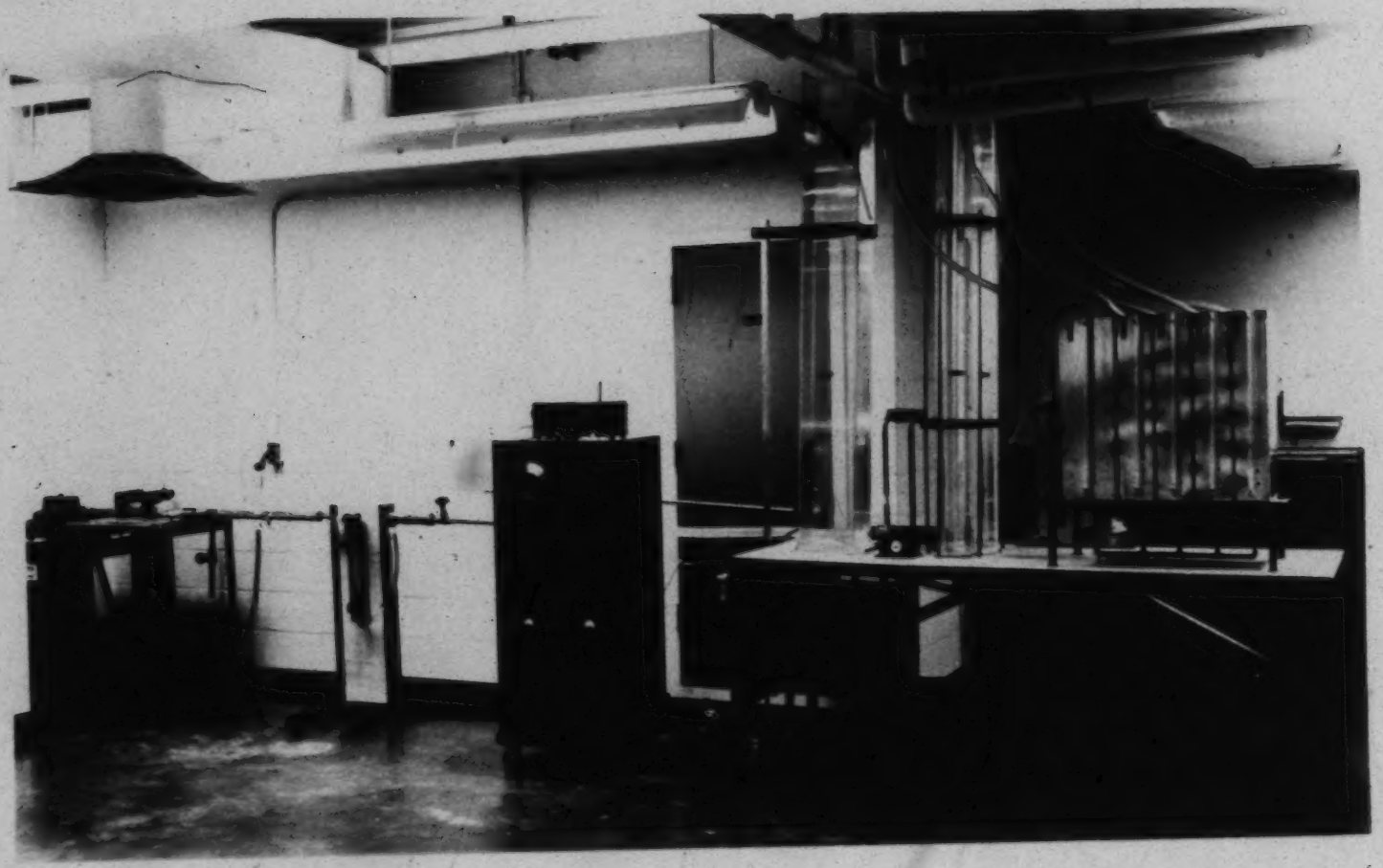

Figure 3.5: Total View on Apparatus

twelve feet in length and as straight and horizontal as possible. The length ratio of the apparatus was

$$L_e = R_o/L = 0.0038$$

as compared to the value of 0.0193 calculated by Dr. Kuchar[5]. The inlet tubing was suspended by twine from a separate stand to approximate the physiological case in that a certain degree of radial movement is possible. In addition, the bifurcation was set on three rolls and levelled.

The constant head tanks were made of plexi-glass and manufactured in the machine shop of the Mechanical Engineering Department of the U. of A. The tanks were designed and located in such a way that the flow lines from the bifurcation to the constant head tanks were all approximately of equal length. The weirs of the constant head tanks were adjusted to the same constant level (See Figure 3.6) to obtain the desired pressure at the bifurcation. It was maintained by measuring with a level set.* Pressure upstream of the bifurcation inlet was measured using a U-tube manometer.

---

* Level set, from the Civil Engineering Department of the U. of A.

twelve feet in length and as straight and horizontal as possible. The length ratio of the apparatus was

$$L_e = R_o/L = 0.0038$$

as compared to the value of 0.0193 calculated by Dr. Kuchar[5]. The inlet tubing was suspended by twine from a separate stand to approximate the physiological case in that a certain degree of radial movement is possible. In addition, the bifurcation was set on three rolls and levelled.

The constant head tanks were made of plexi-glass and manufactured in the machine shop of the Mechanical Engineering Department of the U. of A. The tanks were designed and located in such a way that the flow lines from the bifurcation to the constant head tanks were all approximately of equal length. The weirs of the constant head tanks were adjusted to the same constant level (See Figure 3.6) to obtain the desired pressure at the bifurcation. It was maintained by measuring with a level set.* Pressure upstream of the bifurcation inlet was measured using a U-tube manometer.

---

* Level set, from the Civil Engineering Department of the U. of A.

3.2.2 The Flow Unit

A centrifugal pump*[1] located close to the reservoir (See Figure 3.4 and 3.5) was connected in series with a rotameter*[2], a damping tank (See Figure 3.7) and a pulsation unit. The Calibration of the rotameter is shown in Appendix D. The damping tank was made of three inch internal diameter plexi-glass tube and a height of ten inches. One third of this damper was filled with mixture, so that the remaining air cushion absorbs the waves from the pulsator. A cam-driven piston-cylinder arrangement provided the sinusoidal flow. The cylinder was made of four inch I.D. stainless steel pipe, both ends of which were threaded to facilitate disassembly should any repair or alteration be necessary. The piston was equipped with a leather cup seal and the cam follower was a roller-type. To cover the range of study, as defined by the dimensionless parameters Re, α, and λ, various cams were used.

A variable speed D.C. motor*[3] was used to power the cam. To produce the desired range of pulse rate, a 30:1 worm gear reducer*[4] was installed to transmit power from the motor to the cam. Figure 3.8

---

*[1] Centrifugal pump "Jabsco" bronze self-priming motor pump unit, model 11810-0003, 1/4 H.P. D.C. motor, Electrical Industries Ltd., Edmonton.

*[2] Rotameter, Model 10A 3565A, Max. flow up to 2.7 USGPM, Fischer and Porter Ltd., Edmonton, Alberta.

*[3] 2 H.P., D.C. Motor, Model G.P.-100, General Electric Ltd., Edmonton, Alberta.

*[4] Crofts Model 22 Worm Gear Reducer, Renold Chains Ltd., Edmonton, Alberta.

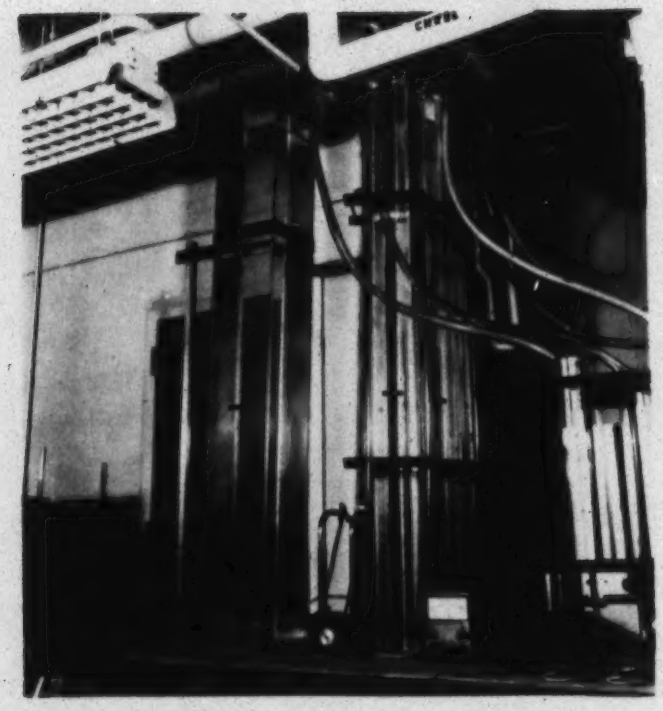

Figure 3.6 Constant Head Tanks

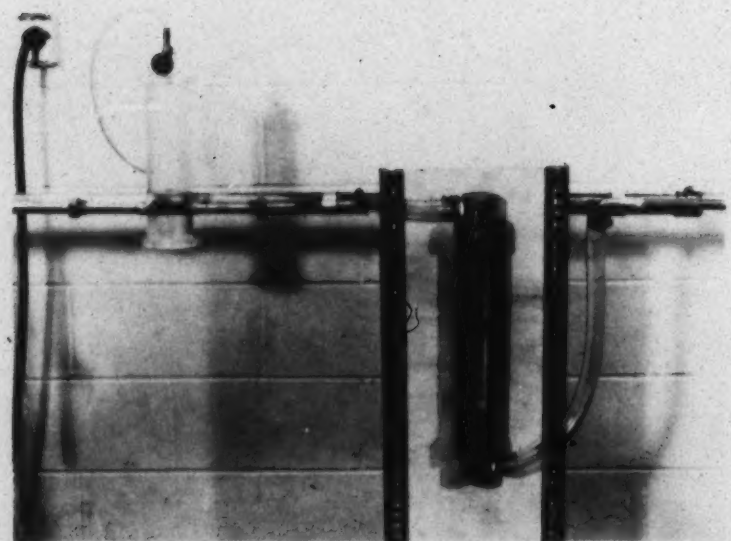

Figure 3.7 Detail View of the Rotameter and Damping Tank

is a photograph of the flow unit and Figure 3.9 is close-up view of the same unit with a typical cam in place.

The flow rate, and consequently Re was controlled by three valves, two (A and B) located at the outlet of the pump, and a third (C) located on the by-pass.

3.2.3 The Flow Rate Measurement Unit

The flow was led from the constant head tanks to graduated vessels by surgical tubing as shown in Figure 3.10. Flow rates were determined in each branch of the aorta by simultaneously closing the drains of the measurement tanks and measuring the elapsed time to collect a given quantity of fluid (varying from 2 to 6 liters).

3.2.4 Test Section

The epoxy resin bifurcation, shown in Figure 3.15 part (H), was used for flow visualization. A detailed description of the development of the artificial aorta follows in the section 3.4.

The inlet to the test section was a 1.25 inch I.D. plastic pipe while the I.D. of the bifurcation was 1.102 inches (2.8 cm.). Each bifurcation branch discharged into a constant head tank (See Figure 3.11). The five tanks were designed to approximate the discharge of fluid from the bifurcation into five infinitely large reservoirs. Four reservoirs were of equal size. The fifth tank was larger because it was connected to the main branch of the aorta. The inlet to each tank was located far from the sidewalls in order to avoid wall effects.

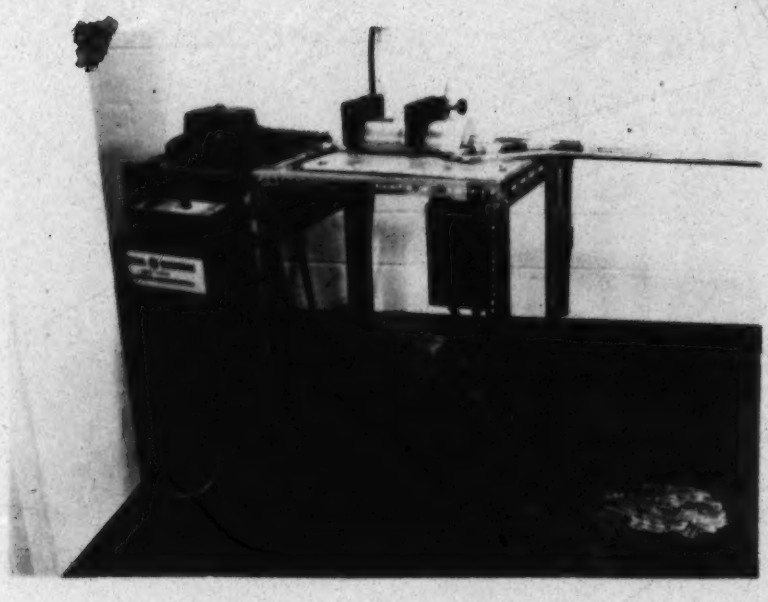

Figure 3. Photographs of the Flow Unit

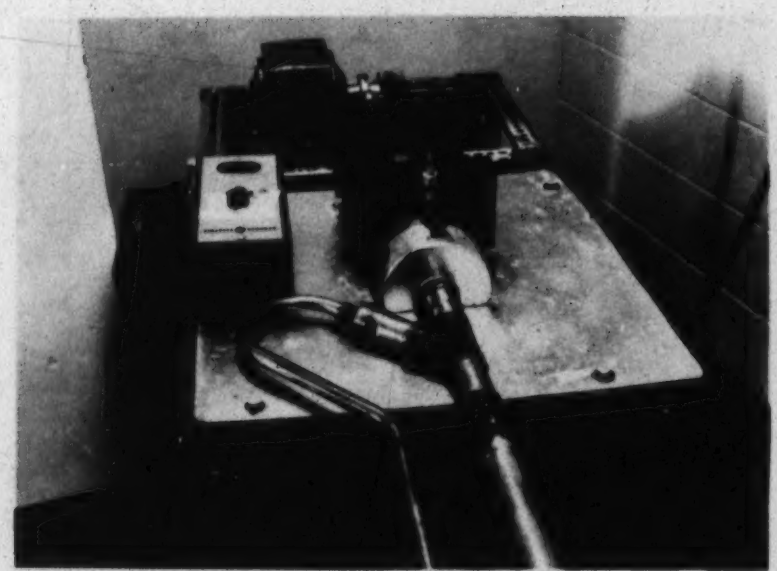

Figure 3.9 Detail View of the Flow Unit

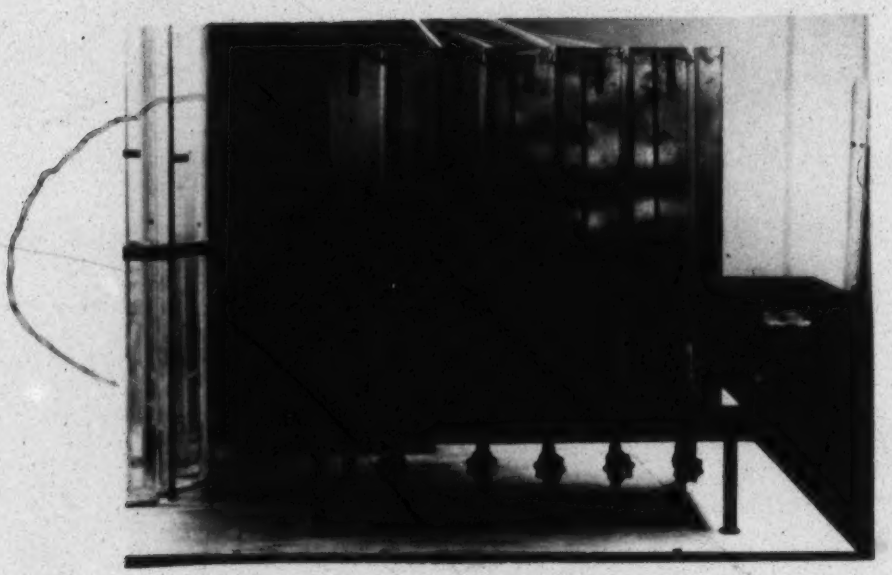

Figure 3.10 Graduation Vessels

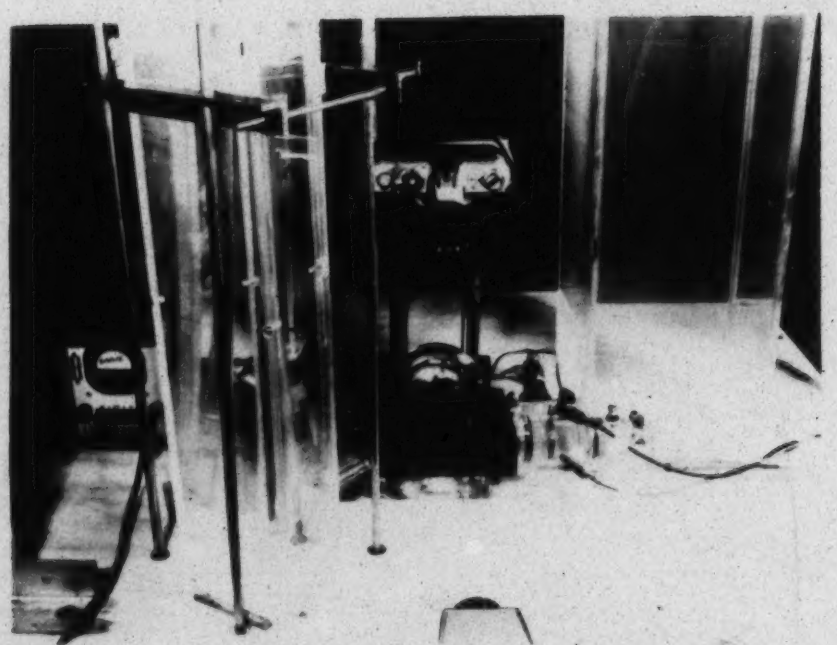

Figure 3.11 Test Section

3.3 The Experimental Fluid

Water was chosen as the experimental fluid for the first part of the experimental work where qualitative observations were made of the flow characteristics in the bifurcation.

For decreasing the surface tension an agent*[1] was added to the water. This was done to ease the flow over a weir, between internal walls of the bifurcation and constant head tanks made of plexi-glass. The viscosity was measured with a Cannon-Fenske viscometer*[2] at 72°F.

For the quantitative experimental studies a mixture of water and glycerol was chosen as the experimental fluid. To simulate more closely real blood flow, the author adopted Weiting's[24] recommendation that a 36.7% glycerol-aqueous solution was a good hydraulic analogue for blood.

3.4 Description of the Development of the Artificial Aorta

A sketch of the aortic arch, giving the relevant dimensions, was obtained from Dr. N.R. Kuchar. Further assistance was received from Dr. Kocandrle, Dr. Kubac and Dr. R.D. Laurenson. As a result of this assistance an artificial aortic arch was designed (See Figure 3.12). This design created a basis for the preparation of a model. Figure 3.13 shows the basic steps in the construction of the aortic arch.

Part A of Figure 3.13 shows the basic part machined to the dimensions of inlet and main outlet branch of the aortic arch. The part B,

---

*1 Photo-Flo 200 Kodak, Edmonton Photo Supply, Edmonton, Alberta

*2 Cannon-Fenske viscometer No. 50J 657, Chemical and Petroleum Engineering of the U. of A.

was machined out of aluminum.

The two halves of the model shown in part C were obtained using part B. Figure 3.14 shows part C in detail. The spaces of the cutting were filled with soldering tin.

The box shown in part D was designed to enable easy removal of the epoxy-resin cast aorta shown in part E. The cast aorta, as shown in part E, was used for production of several paraffin models, part F. These models were repeatedly dipped into the Apex Latex* and dried so that subsequent layers built up a flexible wall of an aortic arch. After drying the paraffin from inside was melted out in hot water. This way a final product of flexible aorta (part G) was obtained with the same inside dimensions as part E.

Part E was worked further by milling, grinding and polishing. The two half bifurcations were finally bolted together and/or sealed with chloroform to form part H, the final test section. This was transparent and used in the visualization experiments. All final types are shown in Figure 3.15. The glass model**(Part I) was used in preliminary studies.

Unfortunately a flexible and transparent model could not be developed because of lack of suitable materials. However, it would be desirable in further studies in this field to develop such an aortic arch.

Generally, the final test model (H) is slightly different from the actual human aorta because all branches are in the same plane, whereas in the human body they are declining in various small angles.

---

* Apex Latex, supplied by Continental Rubber Co. of Canada Ltd., Edmonton, Alberta
**Glass model was made by Glass Shops at U. of A.

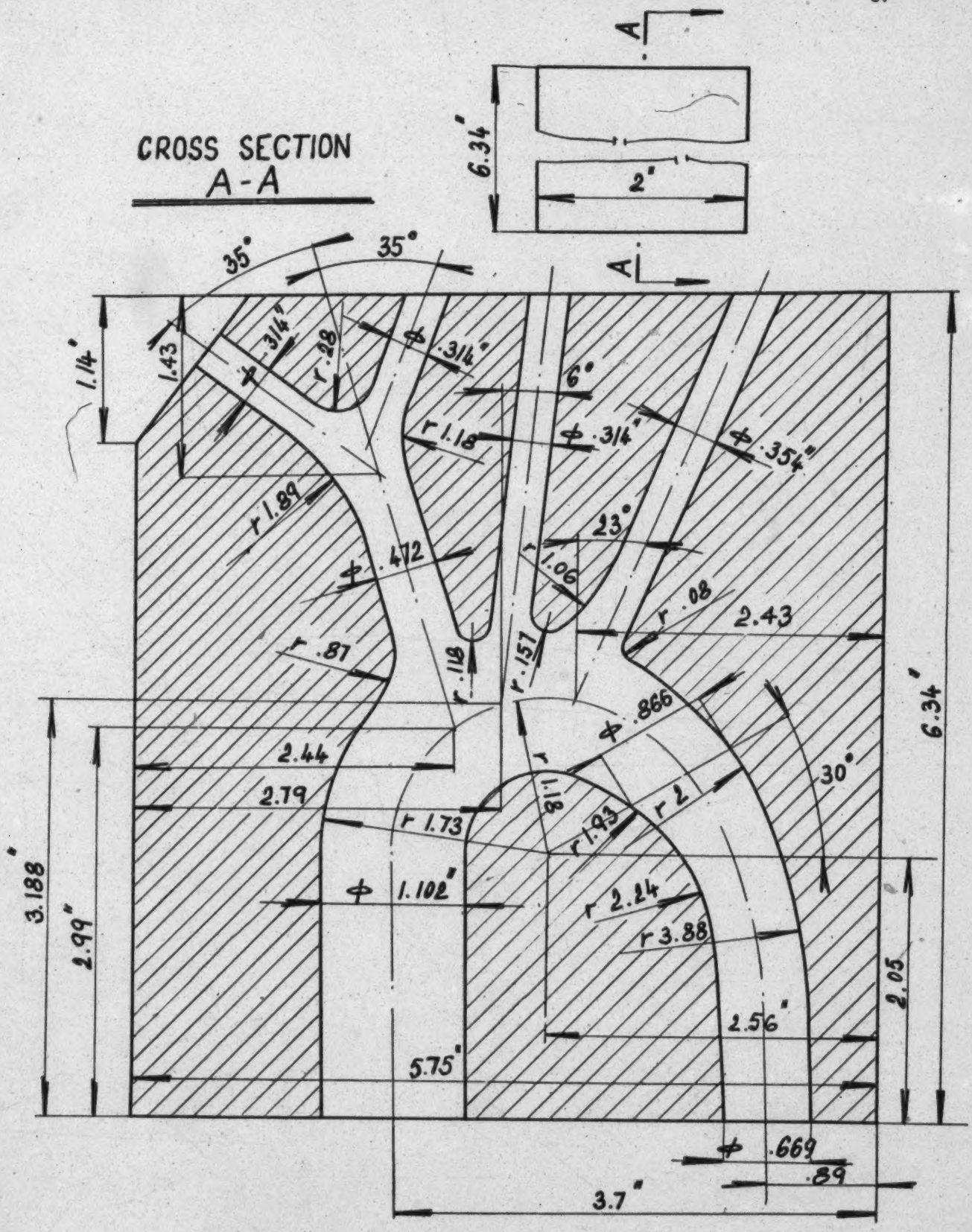

Figure 3.12: Dimensions of the Artificial Aorta

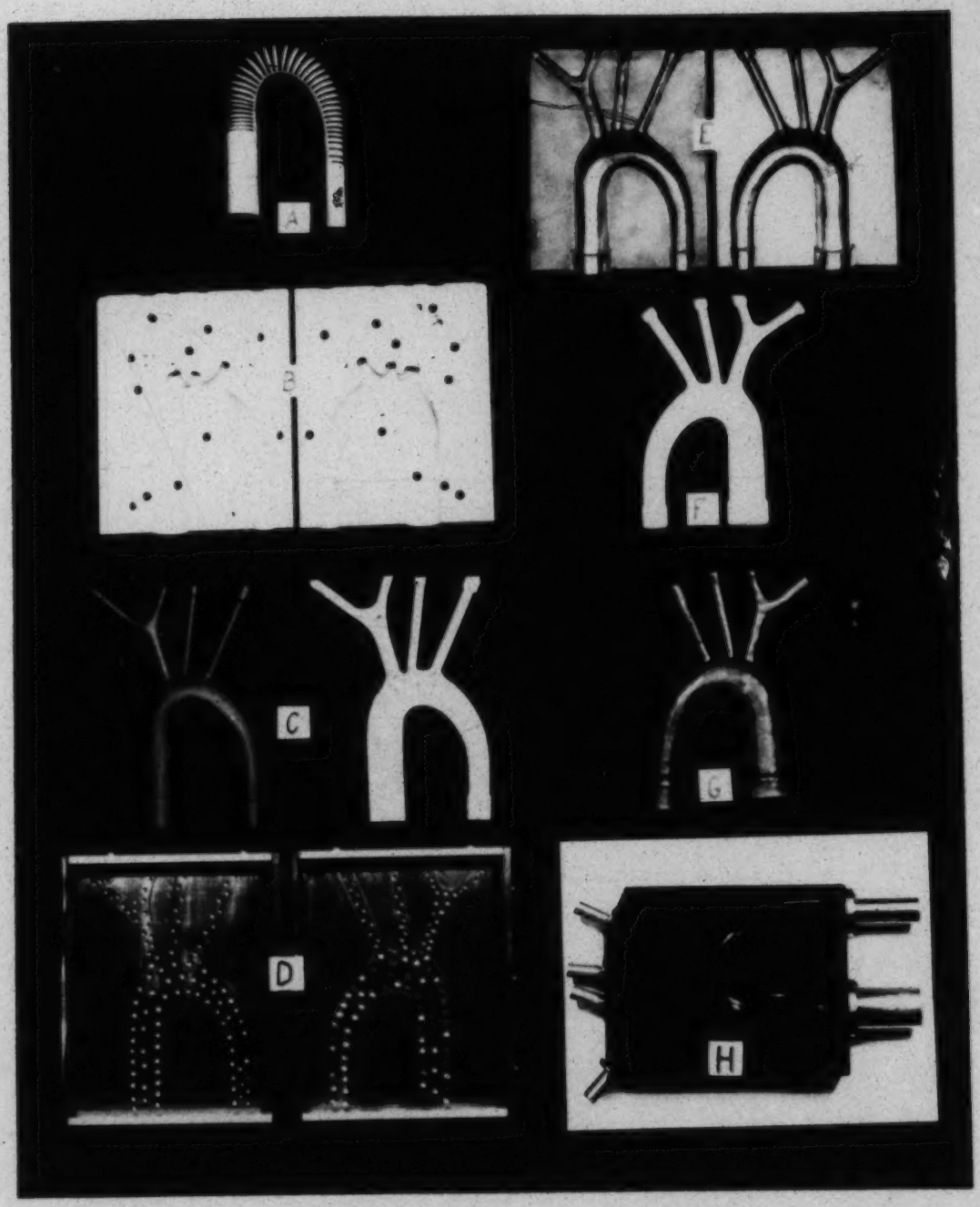

Figure 3.13 Stages in the Development of the Artificial Aorta

Figure 3.14 Detail of Stage C (Figure 3.13)

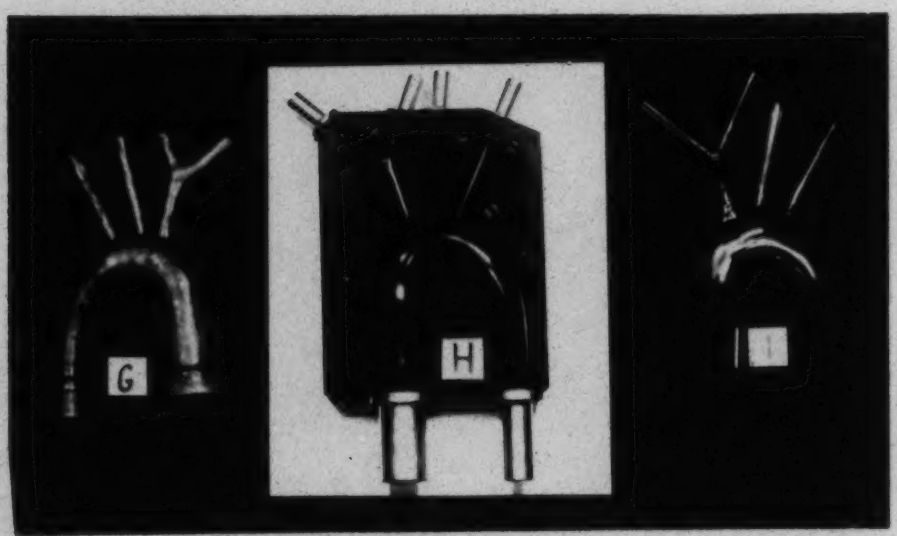

Figure 3.15 Final Types of Artificial Aorta

3.5 Flow Visualization

Resin particles and the "Hydrogen bubble technique" were used by previous investigators for flow visualization (Rodkiewicz - Howell and Rodkiewicz - Roussel). The hydrogen bubble technique appears to be much more efficient. The disadvantage of this method is that water must be used as the experimental fluid. If a water-glycerine mixture is used, the conductance, and therefore, the production of bubbles decreases.

A tungsten wire of 0.002 inch diameter was used as a cathode and a copper ring was used as an anode. The following equations describe the reactions which take place. The oxidation potentials of tungsten and copper are +.12V and -.34V, respectively,

$$\text{Anode: } Cu + 2\ OH^- \rightarrow Cu(OH)_2 + 2\ \bar{e}$$

$$\text{Cathode: } 2\ H^+ + 2\bar{e} \rightarrow H_2\ (\text{gas})$$

$$\text{Water equilibrium: } H_2O \rightleftarrows H^+ + OH^-$$

The hydrogen bubble technique utilizes the electrolysis of water to introduce hydrogen into the flow. These bubbles, formed at the fine-wire cathode are swept off by the flow. The bubbles produced were 0.001 inches in diameter and have a maximum vertical velocity, due to buoyancy effects, of 0.0011 fps and reach a velocity of 98 percent of the fluid velocity within 1 ms, as explained by W. Davis and R.W. Fox[25] according to Rodkiewicz - Roussel.

The wire has, due to its size, an insignificantinfluence on the flow itself. This constitutes one of the best advantages of this method, which also provides a great flexibility to yield qualitative and quantitative results. Qualitative results can be obtained by continuously producing bubbles.

The success of this visualization method is highly dependent on correct illumination. A sharply collimated sheet of powerful light and dark backgrounds are necessary. Other light sources must be suppressed.

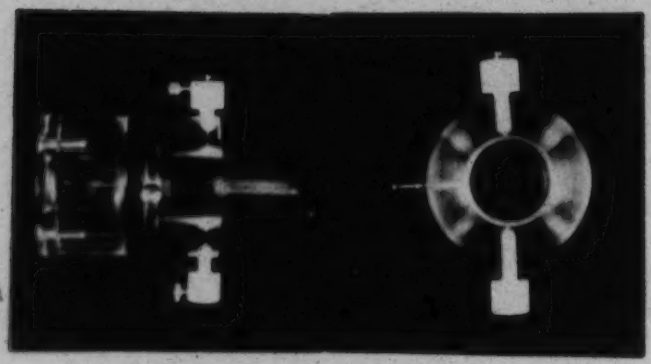

Figure 3.16 Electrodes Housing

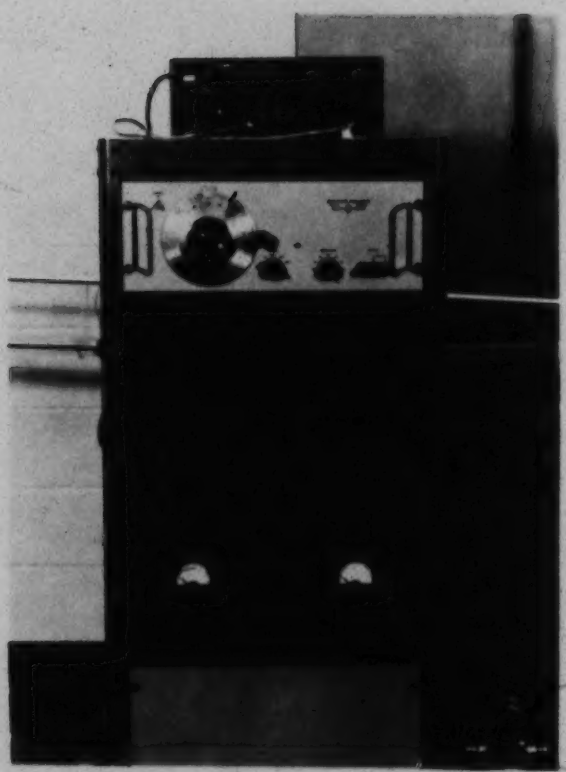

Figure 3.17 Generation Unit for Hydrogen Bubbles

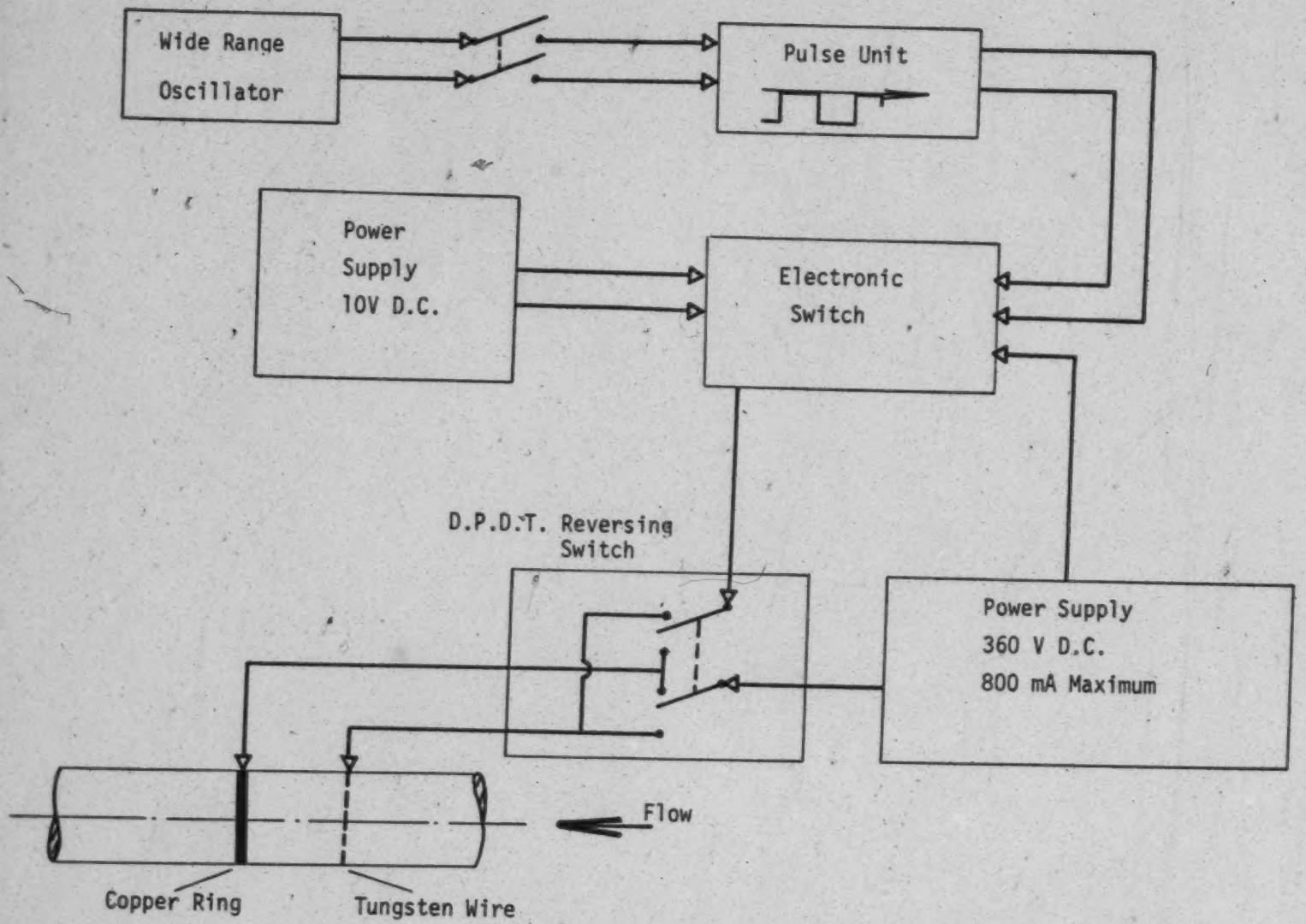

Figure 3.18: Electronics for Hydrogen Bubble Generation

The tungsten wire and the copper ring were built-in to a special electrode housing (Figure 3.16). The electrode housing was designed so that:

1. The wire could be replaced.
2. It could rotate about its axis in order to generate sheets of bubbles in any of the diametrical planes.

The electrode housing was located as shown in Figure 3.11.

The generation unit, which allows the operator to have complete and precise control of the frequency and the duration of the pulse producing the bubbles, is shown in Figures 3.17 and 3.18. From this generation unit the electrolysis DC current is brought to these electrodes. The main part of this generation unit is the constant DC potential power supply*[1].

When the switch is turned on by the pulse generator*[2] which is driven by the Wide Range Oscillator*[3], 360 volts are applied between the two electrodes. The oscillator regulates the frequency of the pulses, while the pulse unit controls their duration. A reversing switch was installed so that the wire could be cleaned.

The photographs of the steady flow streamlines were taken with a reflex camera*[4] loaded with high speed film (Kodak Tri-X Pan, ASA 400). A movie camera*[5] (Kodak 16 mm, Tri-X, Reversal film, Type 7278)

---

*[1] Lambda Regulated Power Supply, Model C 882M, Lambda Electronics Corp.

*[2] Pulse Generator, Type No. 1217 C, General Radio Company.

*[3] Wide Range Oscillator, Model 200 CDR, Hewlett Packard Ltd.

*[4] Canon Camera, Model F Tb, f 1.4; 50 mm.

*[5] Movie Camera, Type: Bolex, H 16 Reflex, 10 mm - wide angle Bolex Lens.

was used for the pulsatile flow studies.

One slide projector (total power 450 W) and one car headlight were used to give a collimated sheet of light in the same plane as the bubble sheet.

CHAPTER IV

EXPERIMENTS, RESULTS AND DISCUSSION

4.1 Experimental Procedure

4.1.1 Preliminary Procedure

A desirable inlet pressure in the bifurcation was maintained by the constant head tanks. The liquid column height was measured with the "level set" instrument and maintained at the equivalent of 115 mm Hg, for all measurements.

At the beginning of each experimental session it was necessary to go through the following procedure:

1. The circulation pump was turned on to circulate the mixture of glycerine and water for at least 30 minutes in order to obtain a homogeneous medium.
2. The dumping tank was filled to approximately 1/3 full with the mixture (2/3 left for air).
3. The density of the blood analogue was checked with the hydrometer and adjusted as required.

4.1.2 Actual Experimental Procedure

1. The appropriate cam was installed.
2. The centrifugal pump was started and the required flow rate was set on the rotameter using valves A and B (See Figure 3.4). Valve B was set approximately and the needle valve A was used for fine adjustment.

3. The pulsatile unit was set at the desired rotational speed and checked with a stop watch. The de-aeration of the pulsator was done using the valve on the top of the pulsator.
4. The drains from the calibrated tanks were closed simultaneously and the elapsed times to gather two liters in tanks 1, 2, 3, 4 and six liters for tank 5 were measured by using five stop watches.
5. The temperature of the solution was measured in the main reservoir. The temperature remained constant at 76°F for the duration of the measurements.
6. The flow rates in each branch Q_1, Q_2, Q_3, Q_4, Q_5, the mass flow ratio γ_1, γ_2, γ_3, γ_4, γ_5 and total flow Q were computed. In general there was at most a $\pm$ 2% difference between the measured flow rate and the flow rate given by the rotameter.

4.2 Photographic Procedure

As mentioned in section 3.2.2 water was used as the experimental fluid to obtain the photographs of the distribution of the

flow through the artificial ascending aortic arch. The conditions under the photographs were taken are as follows:

1. Only one type of cam, of length, l = 0.27 inches was used.
2. Before taking the photographs, the Re was determined (See section 4.1.2 of this chapter).
3. All photographs were taken with the "Cannon" Reflex Camera of the "Bolex" Movie Camera.

4.3 Experimental Results

All of the experimental data are listed in Appendix C.

4.3.1 Steady Flow

All the data has been taken using a mixture of glycerine and water however, photographs were obtained with water alone. The bifurcation inlet pressure was 115 mm Hg. The experimental values were used in plotting Figure 4.1 listed in Table C-4a.

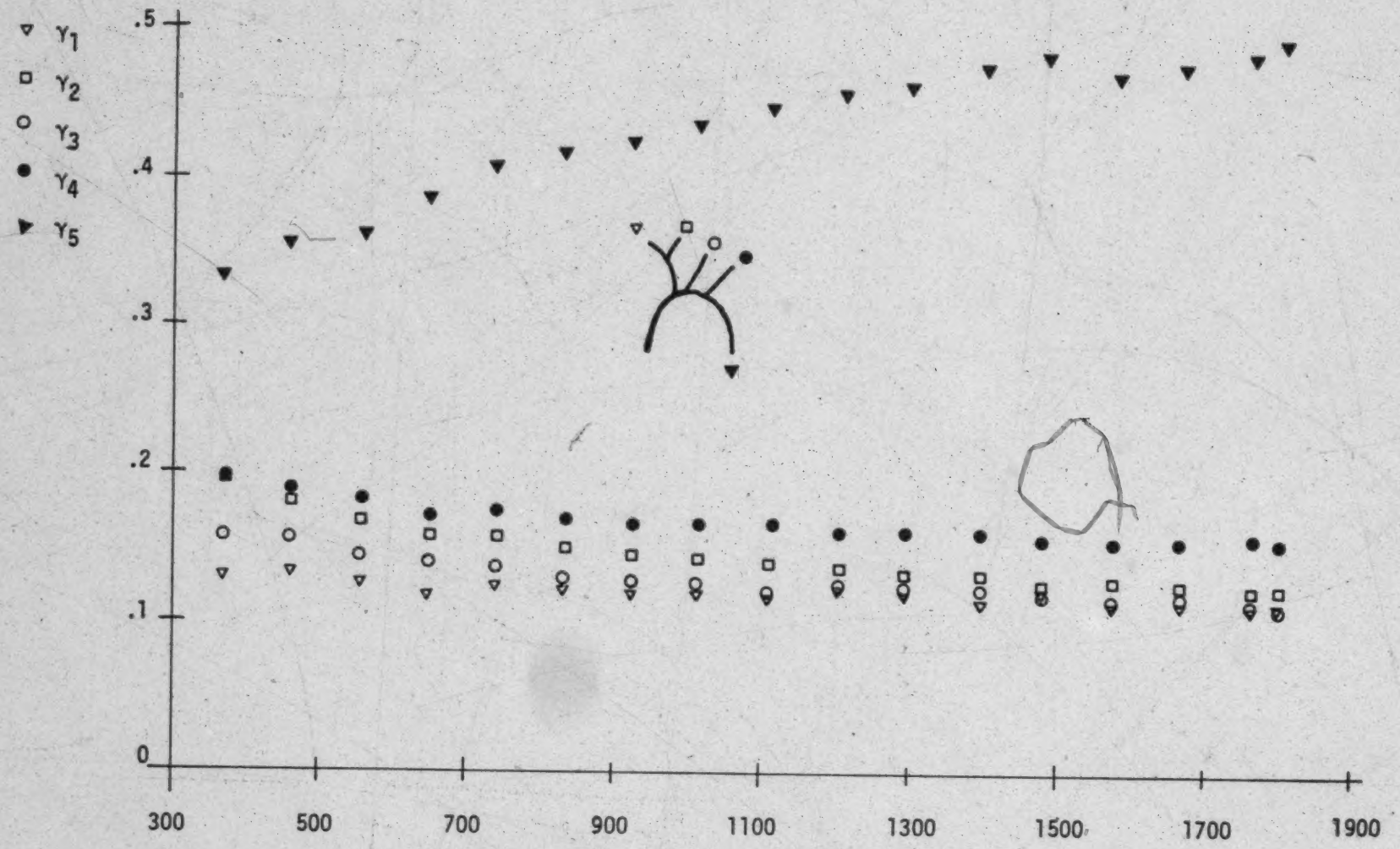

Figure 4.1: Dependency of Mass Flow Ratios on Re,
Steady Flow ~~(Mixture of Water and Glycerine)~~

4.3.2 Mass Flow Ratios as a Function of the Unsteadiness Parameter and the Reynolds Number

The normalized fluctuation component of velocity, λ, was kept constant at a value of one.

The dependence of γ_1, γ_2, γ_3, γ_4, and γ_5 on α was examined at

$$Re = 800, 1300, \text{ and } 1800.$$

The size of cams used (different length of stroke, l), ω, α, and the experimental values obtained for γ_1 γ_2 γ_3 γ_4, and γ_5 are given in Tables C-4.2, C-4.3, and C-4.4. The data of the reproducibility tests are marked with a comma as illustrated in Figure 4.4.

Figure 4.3 shows the relation between γ_1, γ_2, γ_3, γ_4, and γ_5 and α. The Reynolds Number was held constant at 1300 and λ was held constant at 1.5. The experimental data are given in Table C-4.1

4.3.3 Mass Flow Ratios as a Function of the Reynolds Number and Unsteadiness Parameter

The normalized fluctuation component of velocity, λ was kept constant at a value of two.

The dependence of γ_1, γ_2, γ_3, γ_4, and γ_5 on the Reynolds Number was examined at α = 10, 15, and 19. The data in Tables C-4.7, C-4.9 was plotted in Figures 4.4, 4.5 and 4.6.

Figure 4.4 shows the variation of γ_1 (mass flow ratio associated with right subclavian) with Re as a function of α.

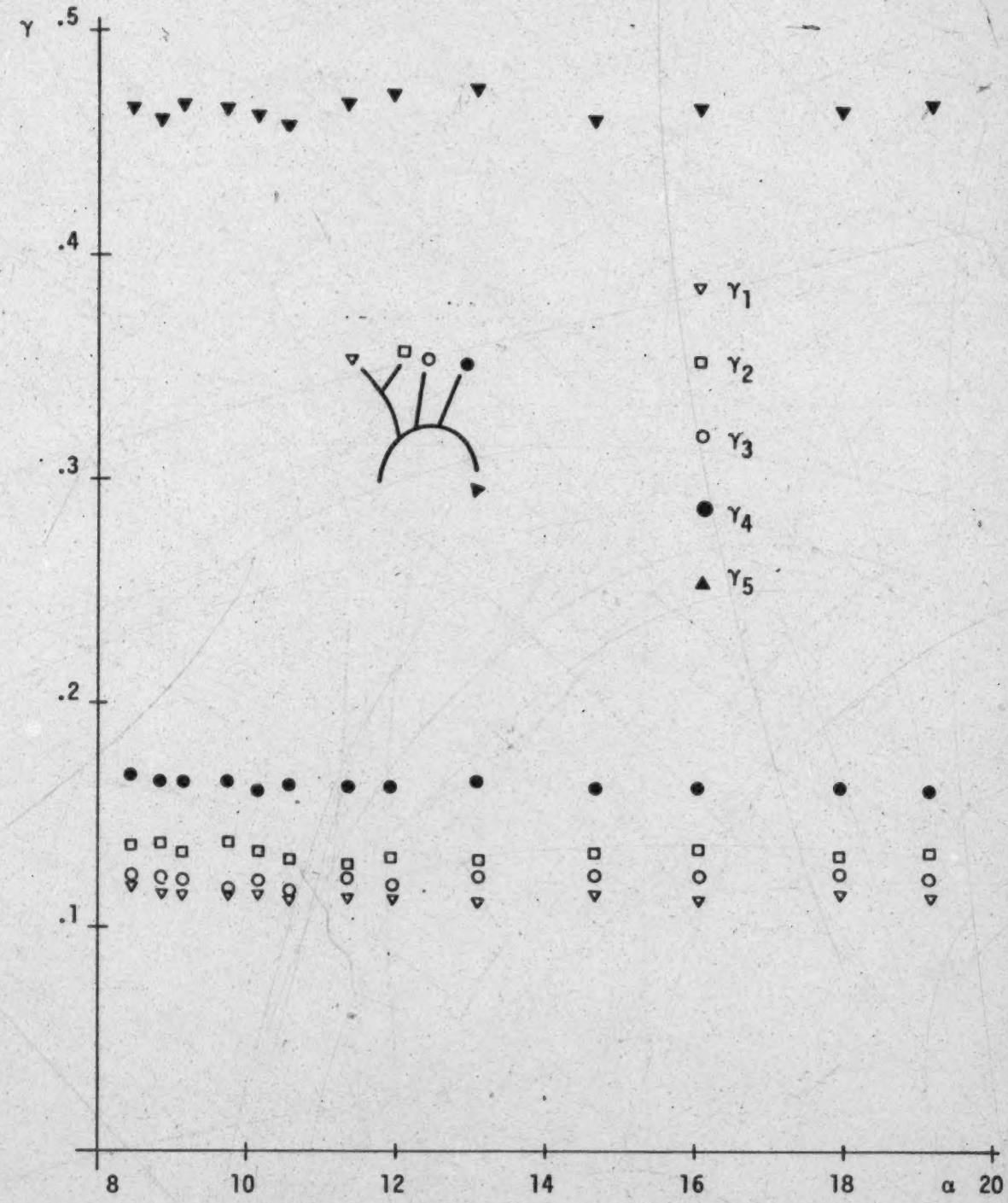

Figure 4.2: Dependency of Mass Flow Ratios on α;
Re = 1300, λ = 1.5.

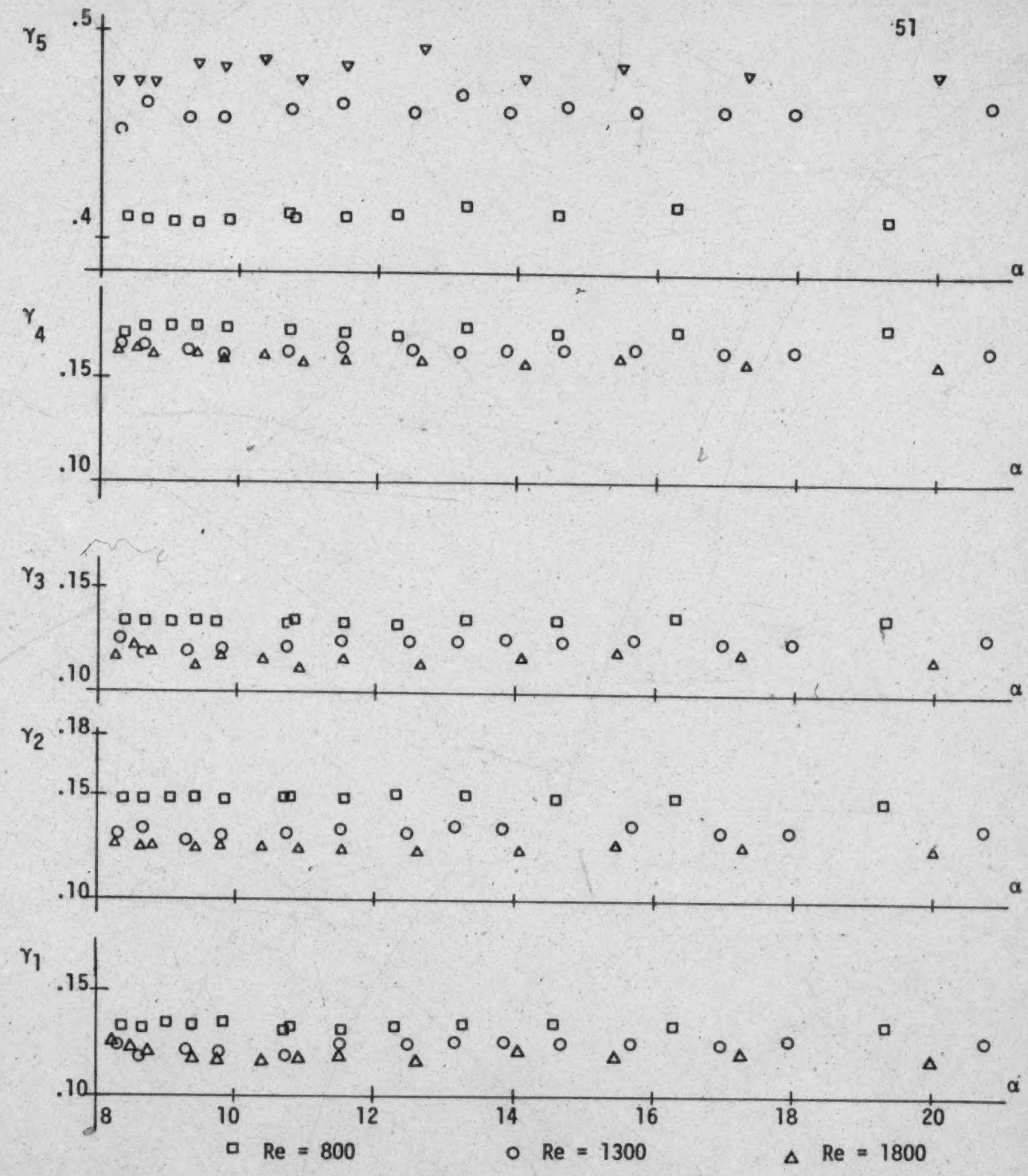

Figure 4.3: Dependency of Mass Flow Ratios on α;
Re = 800, 1300 and 1800, λ = 1.

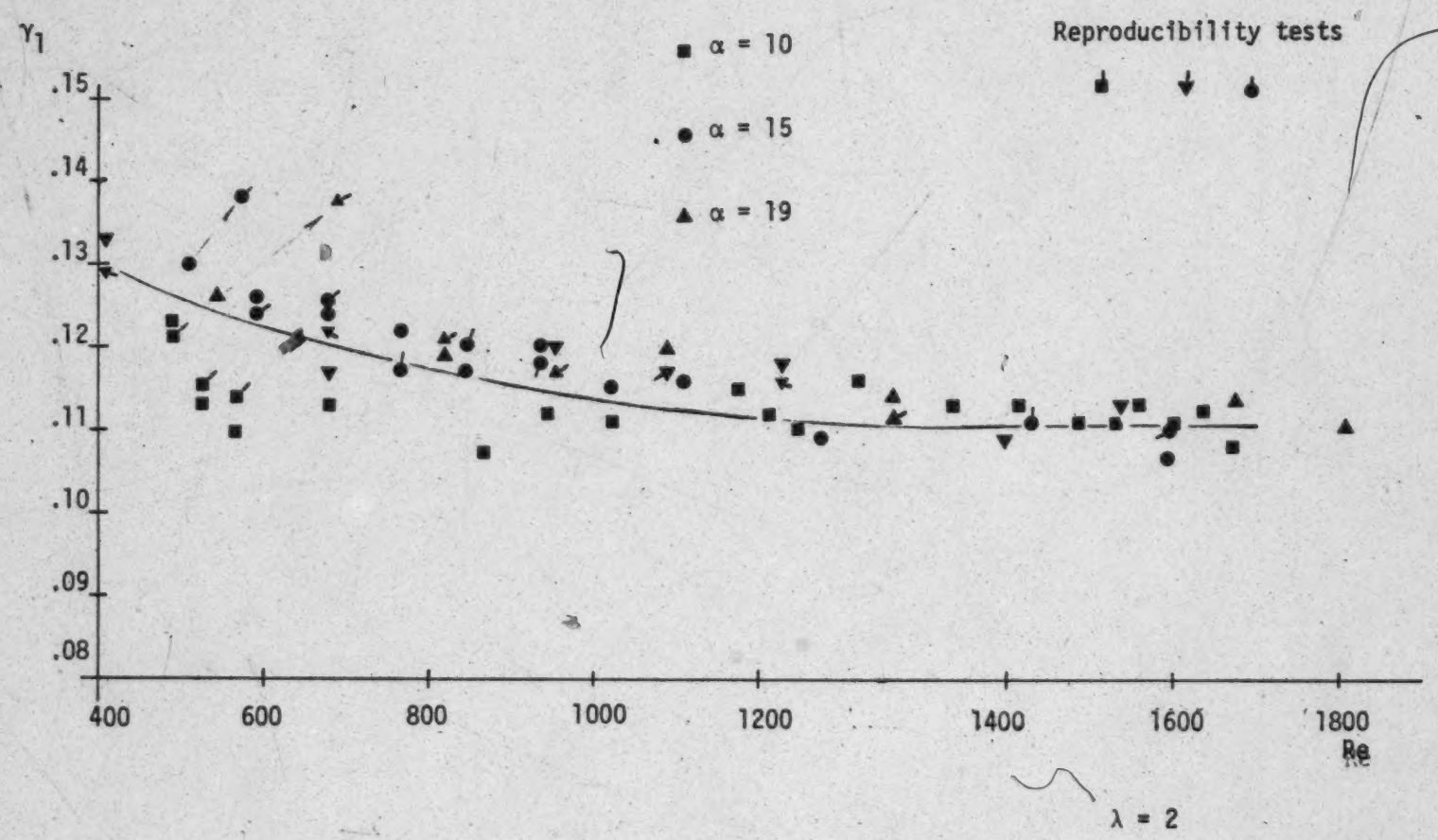

Figure 4.4: Dependency of γ_1 on Re and α, λ = 2.

Figure 4.5 shows the variation of γ_2 (mass flow ratio associated with the right carotid) with Re as a function of α.

Figure 4.6 represents the experimental results for Re and γ_3 (mass flow ratio associated with the left carotid).

Figure 4.7 shows the variation of γ_4, (mass flow ratio associated with the left subclavian) with Re as a function of α.

Figure 3.8 gives the variation of γ_5, (main mass flow ratio associated with the thoracic aorta) with Re, as a function of α.

4.3.4 The Mass Flow Ratios as a Function of the Reynolds Number, and the Normalized Fluctuating Component of Velocity

The unsteadiness parameter was kept constant at $\alpha = 10$. A detailed description of the mass flow ratio and their relation to the branches of the bifurcation is found in section 4.3.3. The dependence of γ_1, γ_2, γ_3, γ_4, and γ_5 on Re was examined at $\lambda = 1$, 1.5 and 2. The experimental data are compiled in Tables C-4.5, C-4.6 and C-4.7.

Figures 4.9 , 4.10, 4.11, 4.12 and 4.13 show the relation of γ_1, γ_2, γ_3, γ_4 and γ_5 to the Re and λ for $\alpha = 10$.

4.3.5 Description of the Flow

Similar characteristics of the flow in an artificial aortic arch can be found in steady flow as well as in the forward flow of

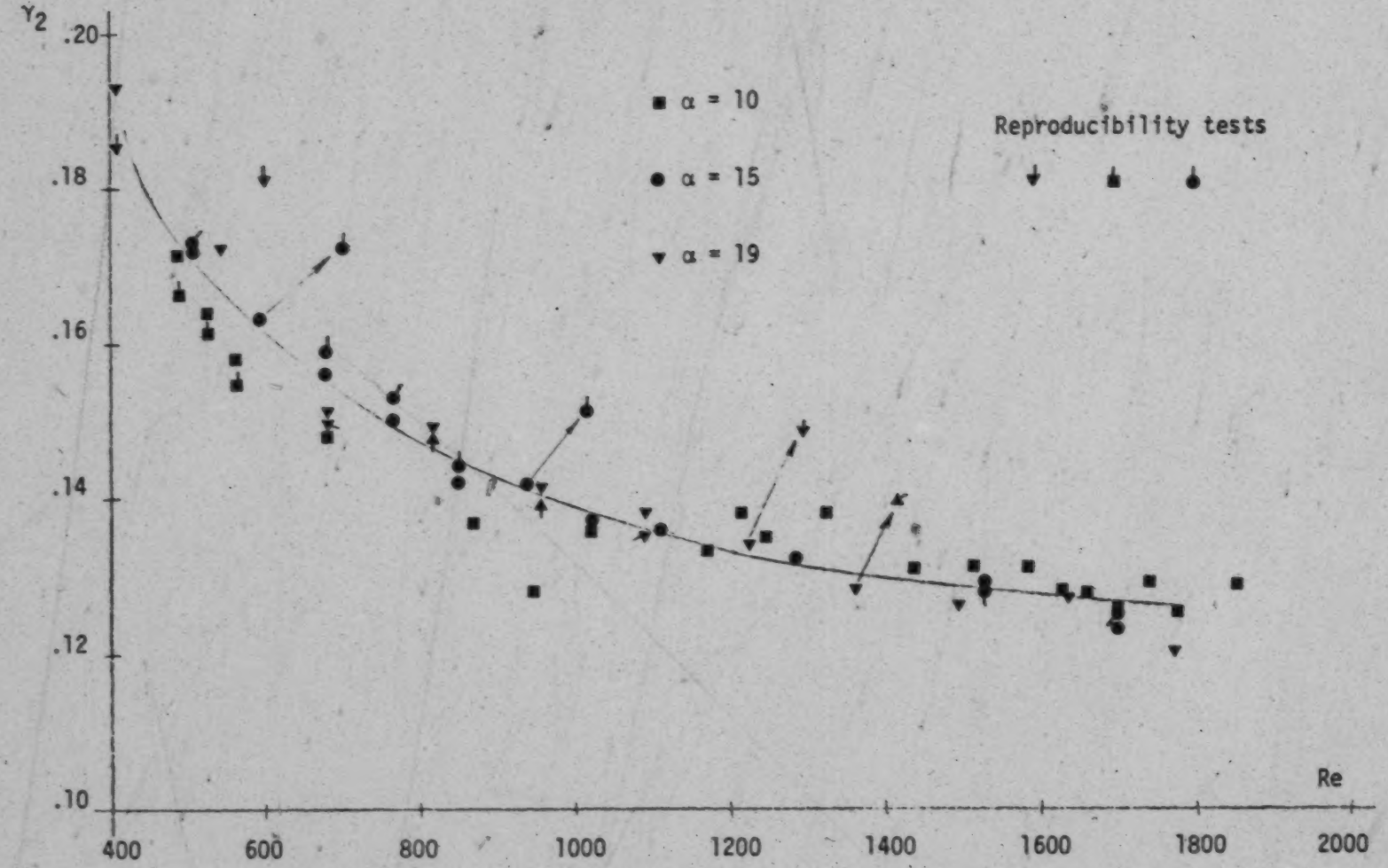

Figure 4.5: Dependency of γ_2 on Re and α, λ = 2.

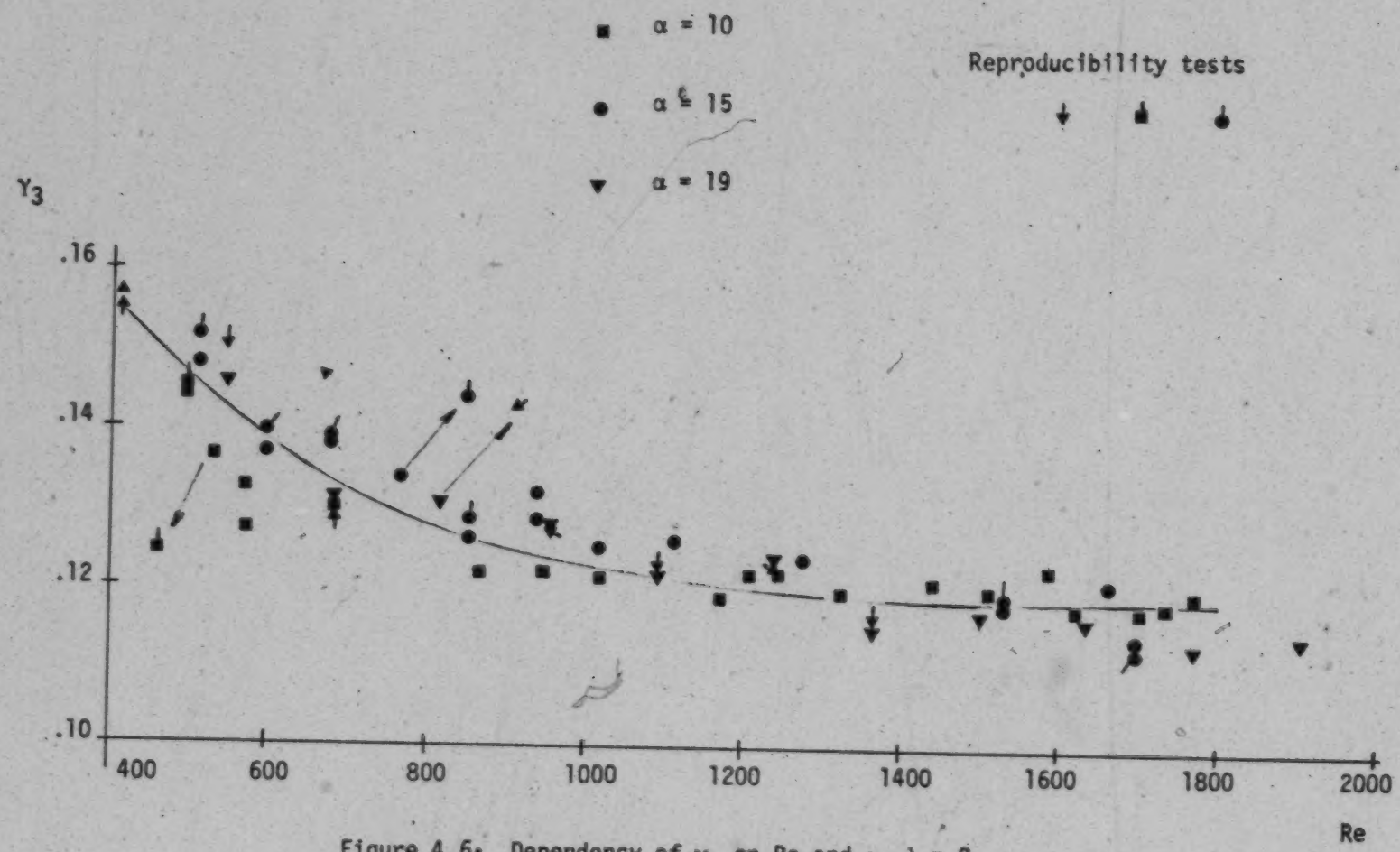

Figure 4.6: Dependency of γ_3 on Re and α, $\lambda = 2$.

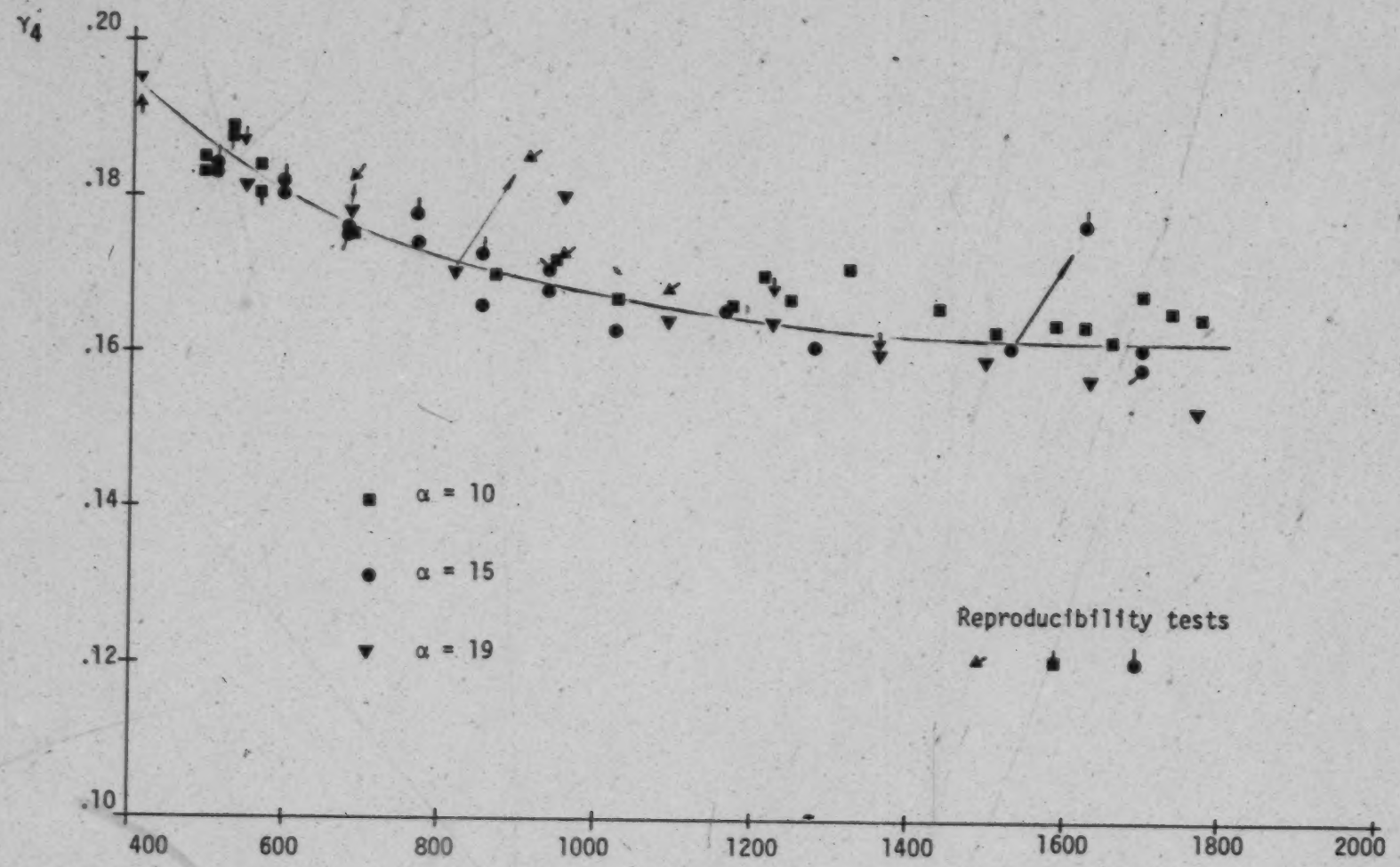

Figure 4.7: Dependency of γ_4 on Re and α, λ = 2.

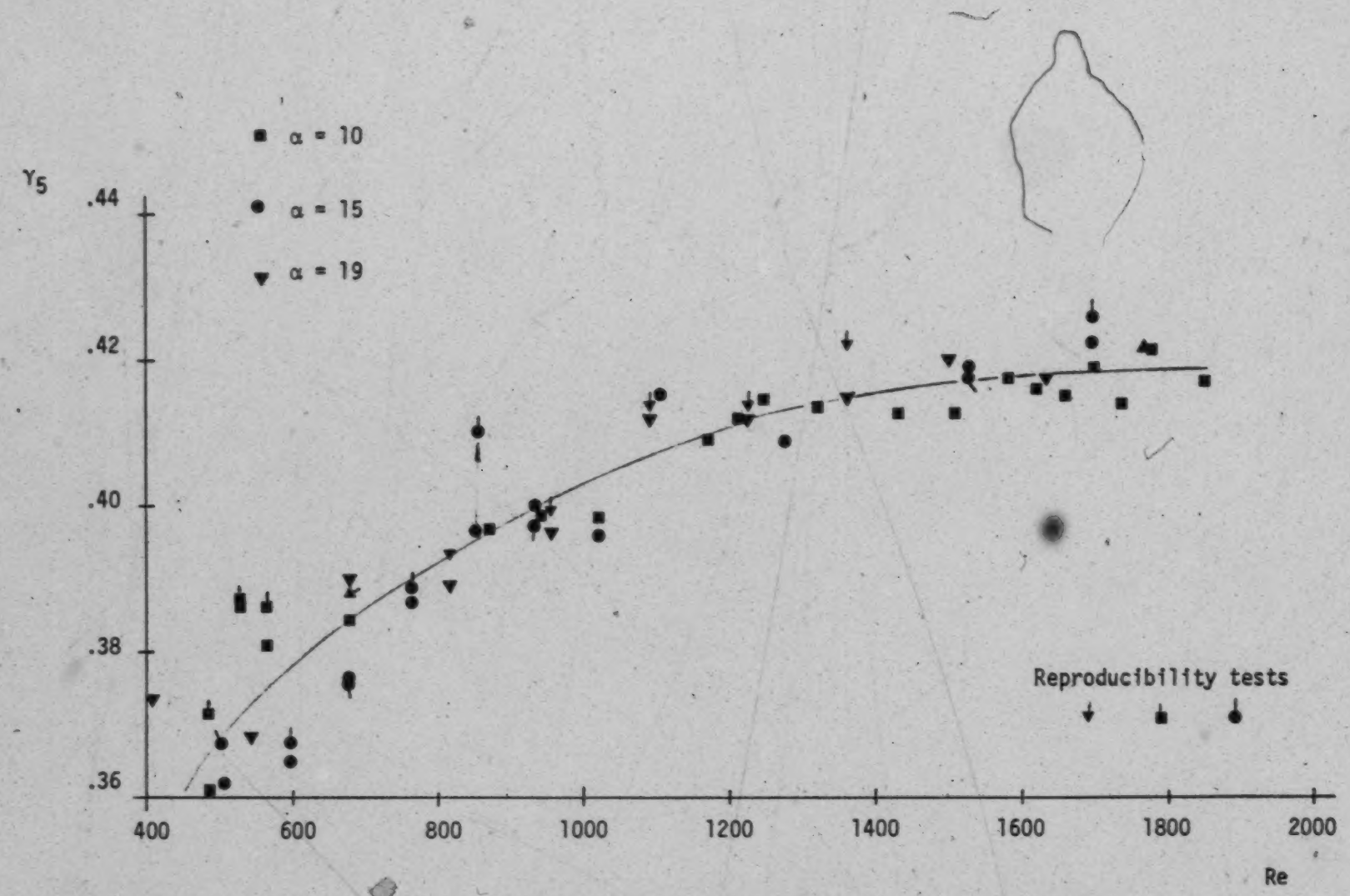

Figure 4.8: Dependency of γ_5 on Re and α, $\lambda = 2$.

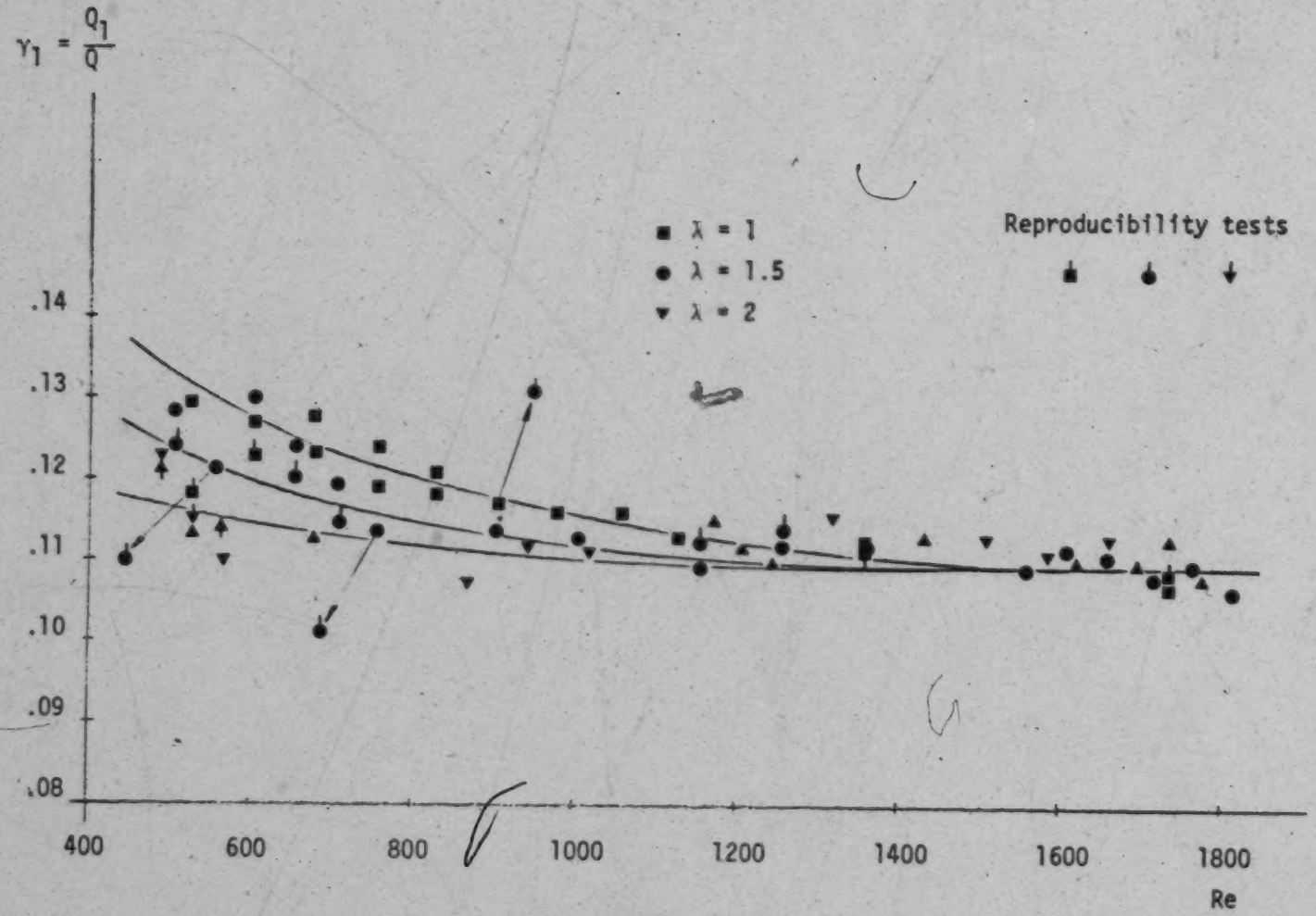

Figure 4.9 : Dependency of γ_1 on Re, α = 10.

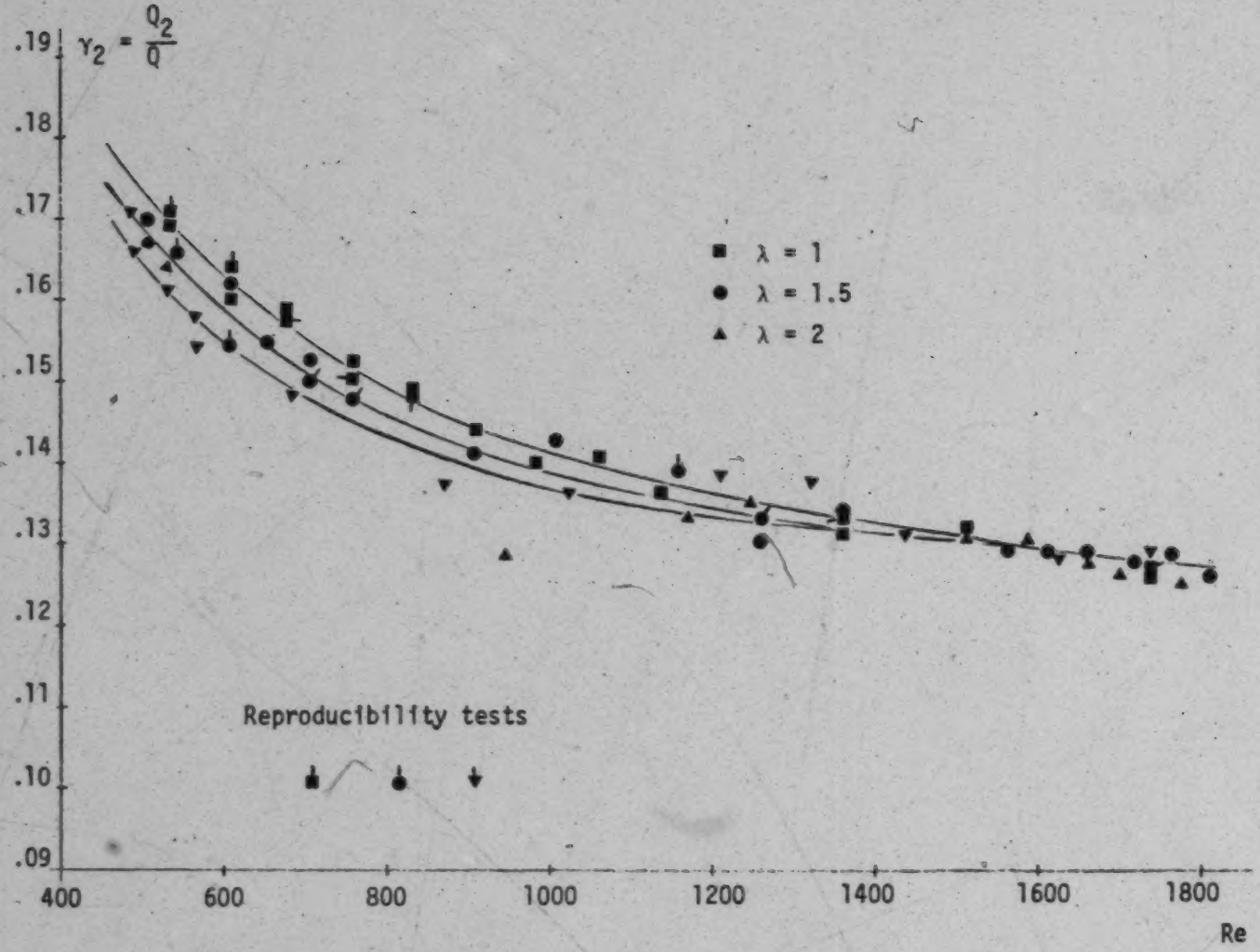

Figure 4.10: Dependency of γ_2 on Re, $\alpha = 10$.

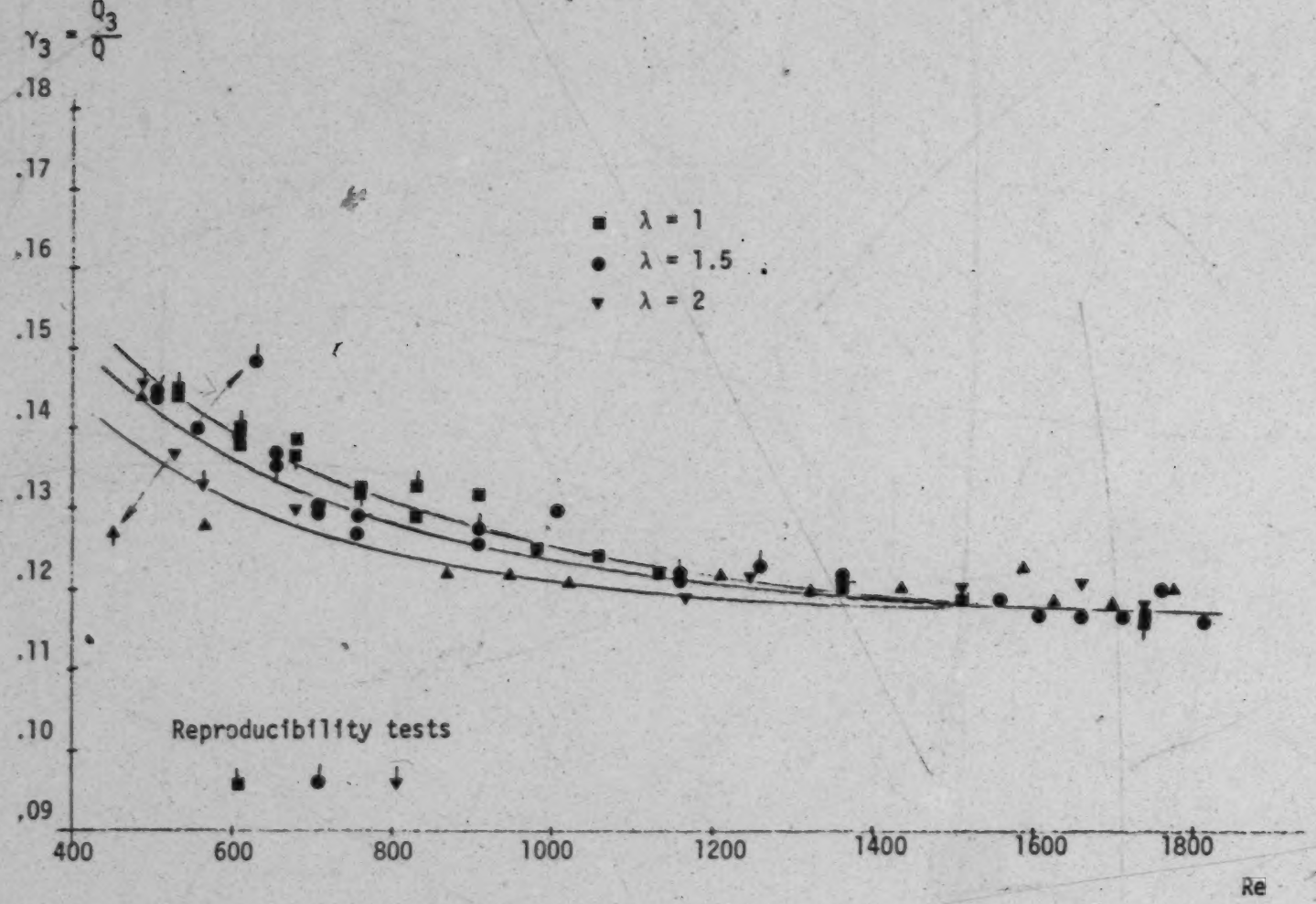

Figure 4.11: Dependency of γ_3 on Re, α = 10.

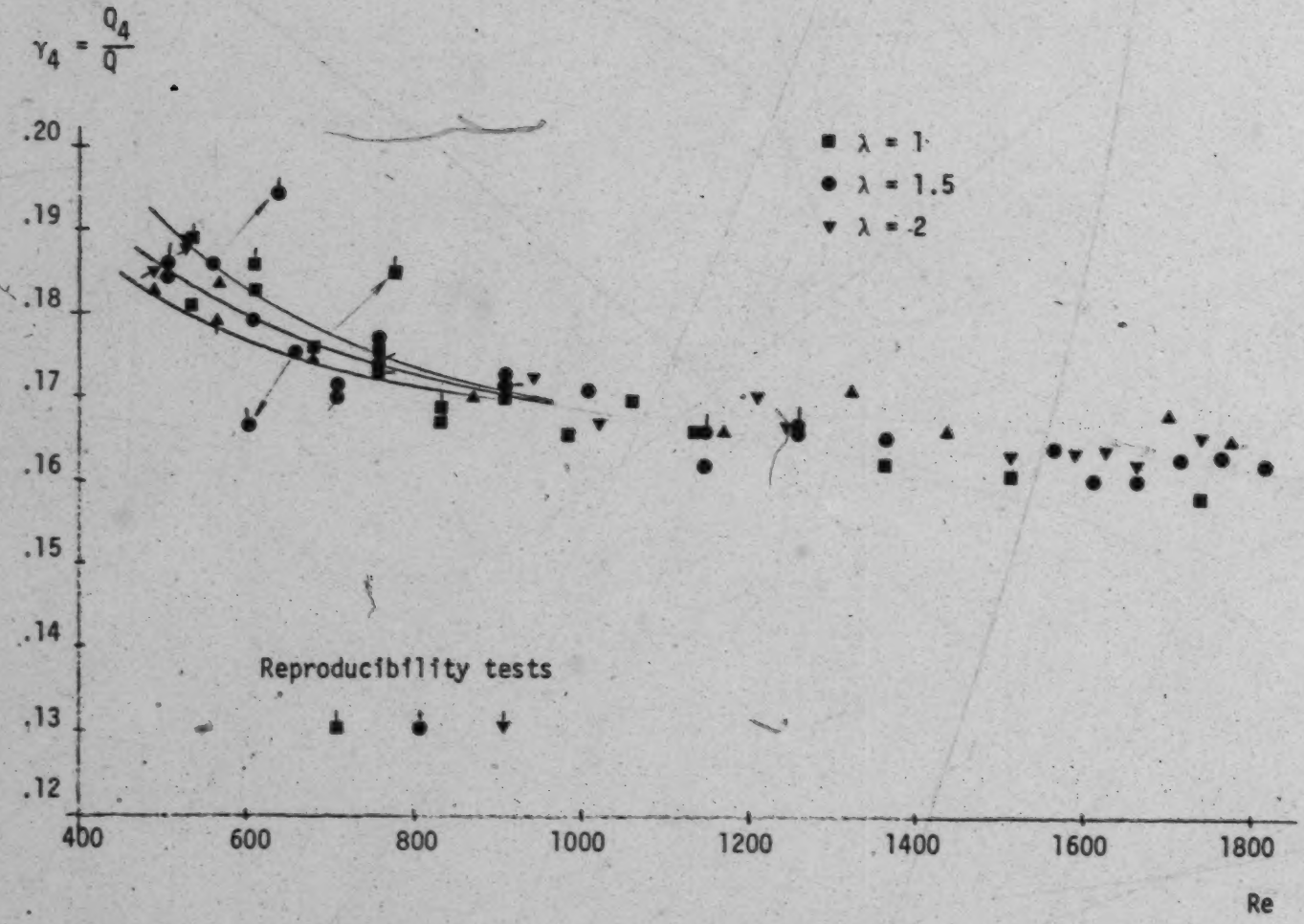

Figure 4.12: Dependency of γ_4 on Re, $\alpha = 10$.

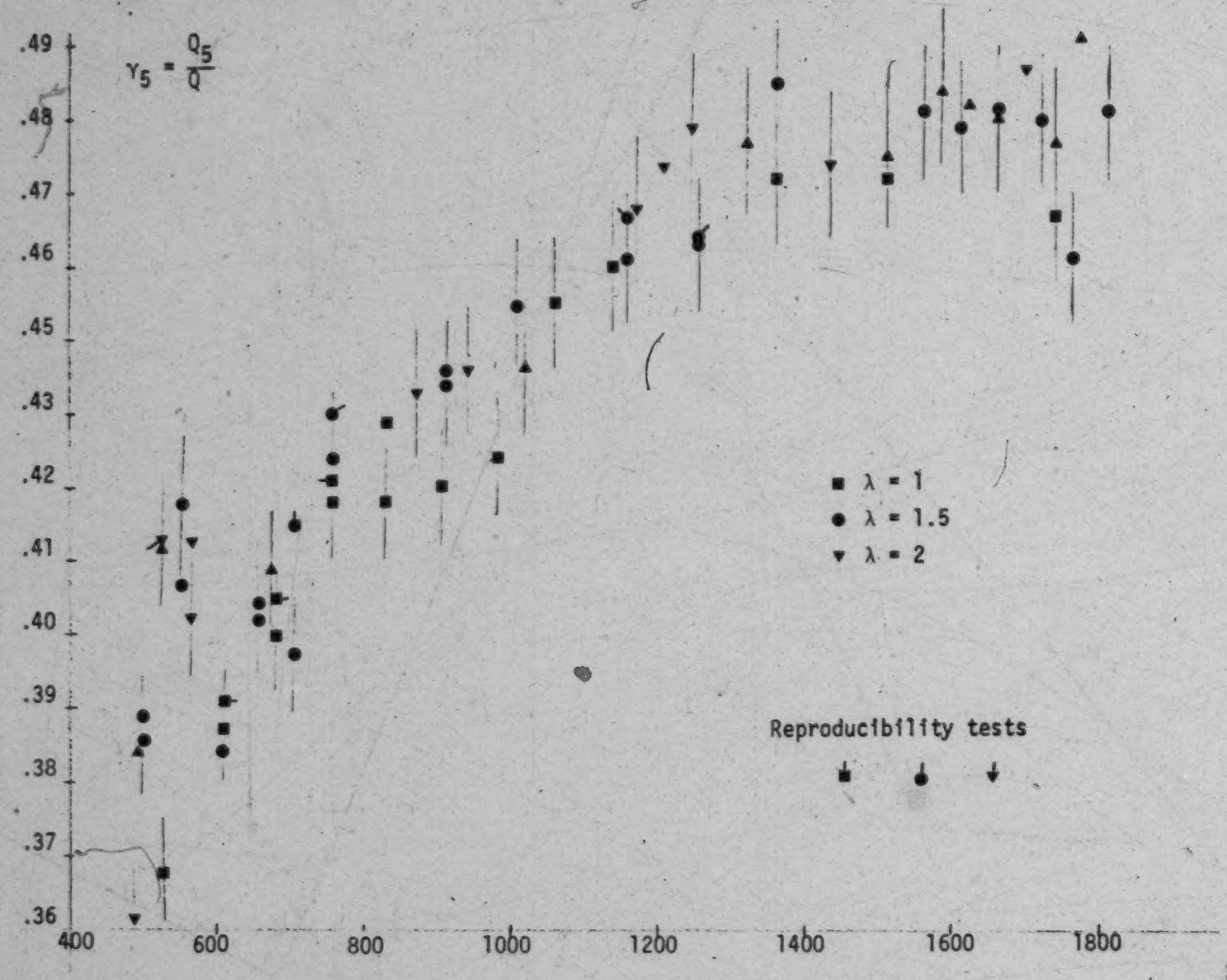

Figure 4.13: Dependency of γ_5 on Re, $\alpha = 10$.

the sinusoidal pulsatile flow, as illustrated in Figure 4.14.

Four separation regions are shown in this sketch. One is in the area where the right common carotid artery divides. Another clearly described region is seen in the area of the innominate artery at the junction of the right subclavian (Branch 1) and the right carotid. Thin separations also occurs in the left carotid and the left subclavian (Branch 3 and 4). These regions, however, though difficult to sight, could not be photographed due to light reflection at the branch edges.

The flow pattern of the back pulsatile flow is shown in Figure 4.15. In this situation the separations regions seen in the steady and forward pulsatile flow, do not appear. However, a separation region does occur on the internal edge close to right innominate artery.

The dependence of the steady flow characteristics on different Reynolds Number, is shown in Figures 4.16, 4.17, 4.18, and 4.19. From Figure 4.20 one can infer the distribution of the streamlines in the aortic arch by the steady flow. The flow distribution in one complete pulse of the pulsatile flow is shown in Figure 4.21.

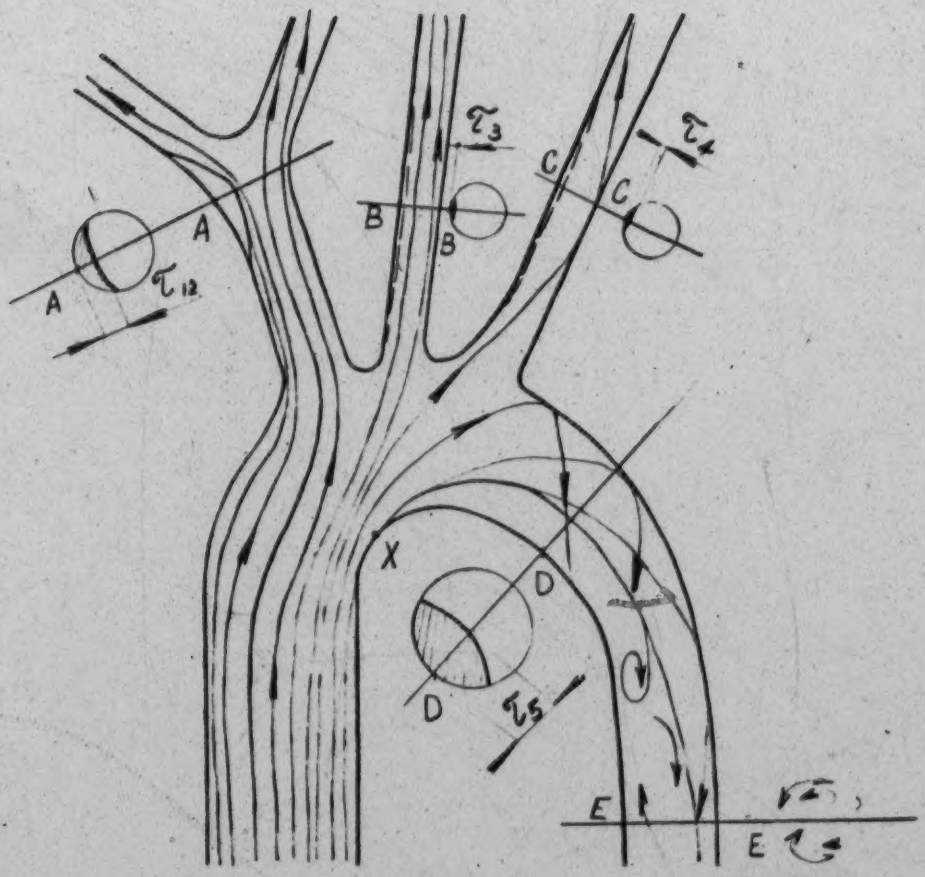

Figure 4.14 Flow Pattern for Steady and Forward Flow by the Pulsatile Flow.

The movie pictures in Figures 4.20 and 4.21 were taken at approximately the same Reynolds Numbers, (Re = 1230, Re = 1180) and show distinctively the different behaviour of steady and pulsatile flow.

The appearance of the double-helicoidal flow in the main branch down stream of the lower aortic arch at different Reynolds Numbers is shown in Figure 4.22.

4.4 Observations and Discussions

4.4.1 Mass Flow Ratio

The study of the diagrams given in Figures 4.1 through 4.13 leads to the following observations:

a. Mass Flow Ratio, γ_1

1. Figures 4.2 and 4.3 indicate that γ_1 is independent of α for a given Re, in range of $10 \leq \alpha \leq 20$, and decreasing function of α and Re in lowest range of α $(8 \leq \alpha \leq 10)$. That is, γ_1 slightly increases as α decreases and γ_1 moderately increases as Re decreases, in this range.

2. In the particular case of sinusoidal flow through the aortic arch γ_1 is a decreasing function of Re (Figure 4.5), for a given α. That signifies if α is increased and λ is kept constant.

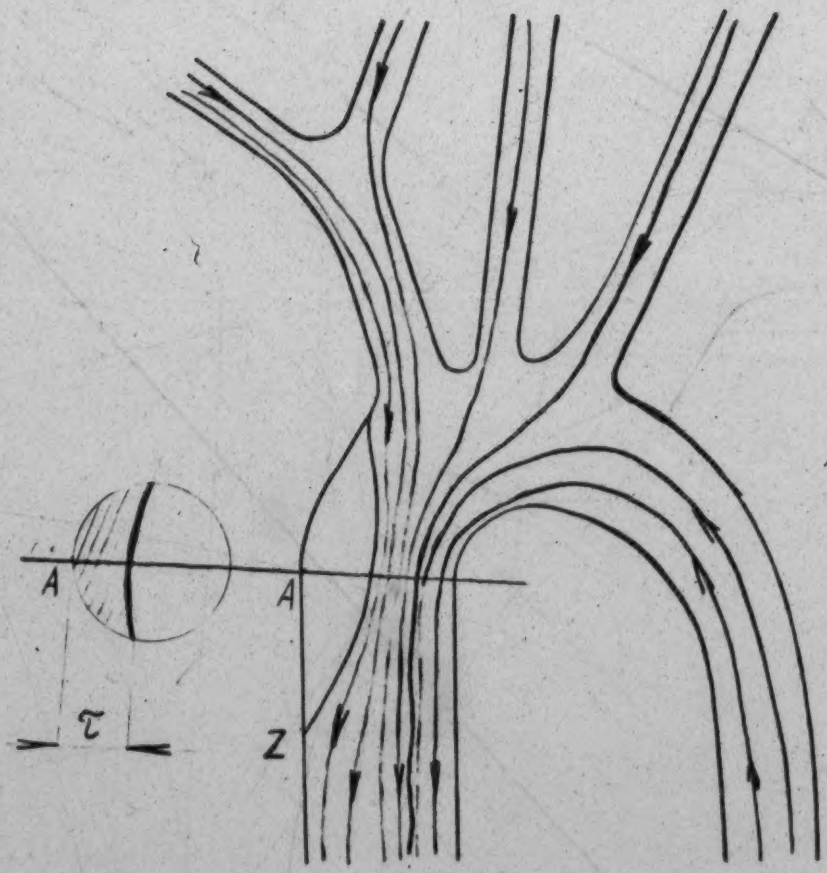

Figure 4.15: Flow Pattern for Back Flow by the Pulsatile Flow.

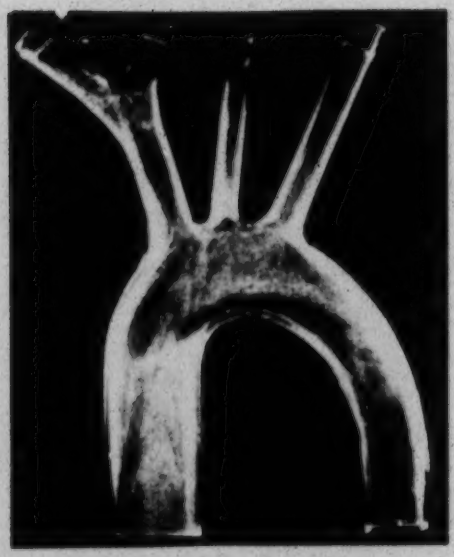

a) Re = 650

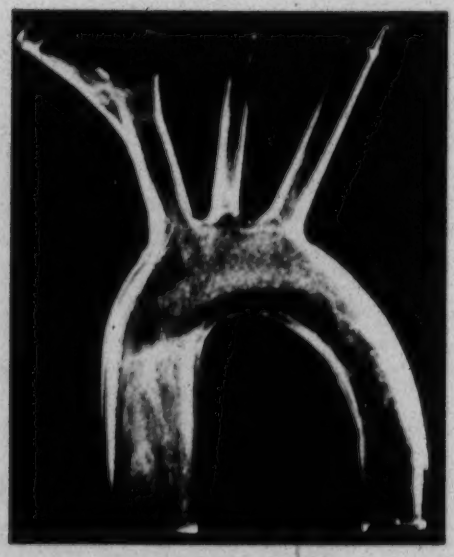

b) Re = 840

c) Re = 1020

d) Re = 1230

Figure 4.16 Steady Flow Characteristics for Various Reynolds Number

a) Re = 1340

b) Re = 1470

c) Re = 1570

d) Re = 1670

Figure 4.17 Steady Flow Characteristics for Various Reynolds Number

a) Re = 1770

b) Re = 1990

c) Re = 2025

d) Re = 2130

Figure 4.18 Steady Flow Characteristics for Various Reynolds Number

a) Re = 2240

b) Re = 2310

c) Re = 2470

d) Re = 2550

Figure 4.19 Steady Flow Characteristics for Various Reynolds Number

Figure 4.20 Development of Steady Flow

Figure 4.21 Development of Pulsatile Flow

a) Re = 1020

b) Re = 1300

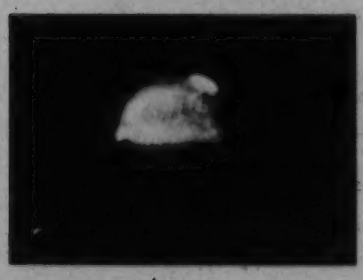

c) Re = 1800

Figure 4.22 Double - Helicoidal Flow in the Main Branch for Various Reynolds Numbers

3. It was found (Figure 4.10) that γ_1 is a decreasing function of Re and the dependence of γ_1 on λ is such that γ_1 decreases with increasing λ, for α = constant, up to Re = 1500. For higher Re, γ_1 is a decreasing function of Re only.

4 For steady flow γ_1 is a slowly decreasing function of Re, (Figure 4.1).

b. Mass Flow Ratio, γ_2

The dependence of γ_2, are similar to those of γ_1 except as follows:

1. For a sinusoidal flow the dependence γ_2 on Re (Figure 4.5) is much stronger than the dependence of γ_1 on Re (Figure 4.4). This may be caused by the fact that the separation region created at the junction of the innominate is forcing the flow to the right carotid, (Branch 2).

2. Figure 4.10 indicates that γ_2 is a decreasing function of Re. Above a certain Re, γ_2 is a decreasing function with increasing λ. The dependence of γ_2 on λ is not as strong as that of γ_1 on λ as shown in Figure 4.9.

c. Mass Flow Ratio, γ_3

The same dependence can apply as in section (a).

d. Mass Flow Ratio, γ_4

The same situation occurs as in section (a) except for the diagram, γ_4 versus Re, (Figure 4.12). Here γ_4 is not so clearly a decreasing function of λ as was the case for γ_1, γ_2, and γ_3. The dependence of γ_4 on λ is not apparent and cannot be determined without further testing.

e. Mass Flow Ratio, γ_5

1. Figures 4.2 and 4.3 indicate that γ_5 is not a function of α for a given Re.

2. For the sinusoidal flow through the main branch of the artificial aorta, γ_5 is not a function of α, and γ_5 is a function of Re only. The velocity fluctuation being kept constant.

3. Figure 4.13 indicates that γ_5 is not a decreasing function of λ as was the case for γ_1, γ_2, and γ_3. The dependence of γ_5 on λ is not apparent and cannot be determined without further testing.

4. In steady flow, γ_5 is a function of Re.

In previous sections, the results were described and the interpretation of the physical meaning can be drawn in the following way as indicated by Dr. Kuchar*.

When the geometry of the bifurcation is a highly curved one, the effect of Dean number, K, will increase with increasing Re.

---

* Private communication between Dr. Rodkiewicz and Dr. Kuchar.

As a result, the centrifugal force will aid in driving blood into the head and arms. The pressure gradient at the centre zone of the aortic arch will create secondary flow from the internal to the external wall of the aortic arch. This occurs where the first three branches (innominate aorta, left carotid, and left subclavian) are located.

This would indicate that the flow ratios of the first four branches (the upper extremities) decrease with increasing Re, at the expense of the flow ratio of the main branch. In summary it appears that as the Reynolds Number increases the mass flow ratios of flow to the first four branches decrease and the flow ratio of the main branch increases correspondingly. That is, as the total blood flow is increased a smaller portion is diverted to the upper extremities.

4.4.2 Separation Regions

a. Separation Created by the Steady Flow and Forward Pulsatile Flow

In this particular case, the photographs and observations clearly prove the existence of four interdependent separation regions:

1. The largest separation region is in area of internal wall of upper and lower aortic arch and continues into or ends in the vicinity of the upper thoracic aorta. The termination of this region is difficult to determine.

It can be seen from Figures 4.17 through 4.21 that by increasing the Reynolds Number, point X of the separation (Figure 4.15) is moved further along the internal wall upstream and its thickness τ_5 becomes greater. The cross-sectional shape of the separation region could not be determined and the shape shown has been assumed. Observation of the secondary flow however seems to indicate a profile of this shape.

2. The other recognizable separation occurs in the area of junction of the innominate. From the photographs mentioned above it can be found that by increasing the Reynolds Number the point Y of the separation moves further along the wall of the innominate upstream, and the thickness τ_{12} becomes larger. The tail of the separation moves the same as point Y, to the upstream with increasing Re.

3. The two smaller separation regions appear in branches three and four on the right walls of these branches (Figure 4.14 and 4.15). The separation thicknesses τ_3 and τ_4 are so small that no measurement was possible. In general only qualitative results could be obtained due to smallness of the regions.

b. Separation Created by Back Flow of the Pulsatile Flow

During back flow all the previous described separations disappear and a new separation region is created as shown in Figures 4.16 and 4.22. It was found that by increasing Reynolds Number, the

Point of separation Z is moved downstream and the separation region became more convex.

A vortex formation was seen in the area at the end of the main branch. Its occurrence can be seen in Figure 4.21.

Inside the main branch and branches of the left carotid and left subclavian, the double-helicoidal flow was observed. In the area downstream of the lower aortic arch, as the flow entered the head tank, photographs were taken perpendicular to the cross-section of the main branch. In this particular cross-section the axis of double-helicoidal flow is oriented as shown in Figure 4.22 or as sketched in Figure 4.14 (Section E-E). This kind of flow is typical of flows in curved pipes as explained by H. Schlichting[16].

4.5 Limitation of the Apparatus

Several test runs were repeated to check if the test runs were reproducible. The results were as follows:

The results of the check of the experimental sensitivity were found to agree to within $\pm$ 2%.

The reproducibility is directly proportional to the care taken to obtain precisely the same level for all five constant head tanks, because the flow through the bifurcation is highly dependent on the resistance in each branch.

The visualization technique becomes useless below Re = 600, due to the growing importance of the buoyancy effect on the hydrogen bubbles.

CHAPTER V

CONCLUSIONS

5.1 Summary

For the physiological range of unsteadiness parameter, Reynolds Number, and for normalized velocity fluctuation, the experimental findings can be summarized as follows:

1. The mass flow ratio, γ_1 is:
   a. Not a function of α for a given Re in range of $10 \leq \alpha \leq 20$.
   b. Inversely proportional to α in the lowest range $(8 \leq \alpha \leq 10)$ for a given Re.
   c. A decreasing function of both Re and λ, for α = constant up to the range of Re = 1500. For increased Re, γ_1 is a decreasing function of Re only.
   d. In steady flow, a decreasing function of Re.
2. The mass flow ratio, γ_2 has same dependences as γ_1 except as follows:
   a. The dependency of γ_2 on Re is more pronounced. This might be caused by the separation created in region of junction of the innominate.
   b. The dependency on λ, is not so strongly indicated.
3. The mass flow ratio, γ_3 has the same dependences as in case of γ_1.

4. The mass flow ratio γ_4 has the same dependences as γ_1 except the dependence on λ is not apparent and cannot be determined without further testing.
5. Results of the other mass flow ratios indicate a dependence on λ, however Figure 4.13 shows no discernable trend; perhaps due to the limitation of the experimental sensitivity. It is shown, however, that γ_5 is a function of Reynolds Number. The mass flow ratio γ_5 is not a function of α at least in range $10 \leq \alpha \leq 20$ for a given Re.
6. There exist four interdependent separation regions in the steady and forward pulsatile flows.
7. With back pulsatile flow, all separations mentioned above seem to disappear and are replaced by one located at the outside wall just before the innominate branch.
8. A visualization technique proved the vortex formation observed in the separated region of the main branch under lower aortic arch.
9. The double helicoidal flow has been observed in branches 4 and 5 in steady and forward pulsatile flows.

5.2 Suggestions for Further Work

1. It would be of interest to obtain clearer photographs and movie pictures so that better visualization of the distribution of the flow could be observed. It might be interesting to magnify proportionally the artificial

aorta and improve the illumination (for instance from all four sides) to remove reflected light from the side walls branches.

2. Repeat the same tests with the artificial flexible aorta (a flexible aorta was developed by the author with the assistance of Mr. Golls) and results compared with those obtained in this thesis.
3. Repeat the tests performed using redesigned aortas with different geometry, mainly with different curvature of aortic arch to study how the curvature would influence the dependence of mass flow to the branches, (Dean number, K; or Modified Dean number, Km, versus mass flow).
4. Tests should be performed which will better simulate conditions for "real" flow through the aorta. This data obtained can then be compared with results obtained from sinusoidal flow.
5. Finally simulate the experiments "in vitro" and compare the results with the artificial one. To simulate the "real" flow in aorta, the author suggests using the same constant head tanks, graduated vessels and the reservoir, as used in this experiment. The artificial left ventricle with its artificial valves put in series as follows: constant head tanks from overflow to graduate vessels - reservoir - the free flow lead into the artificial left ventricle from aorta back into the bottom of constant head tanks.

REFERENCES

1. F.R. Winton and L.E. Bayliss, "Human Physiology", Third edition, Philadelphia, Blakiston, 1948.
2. J.R.A. Mitchell and C.J. Schwartz, "Arterial Disease", Blackwell Scientific Publications, Oxford, 1965.
3. I.G. Porjé, J. Karnell and B. Rudewald, "Haemodynamic Studies of the Human Ascending Aorta During Narcosis and Angiocardiography", CARDIOLOGIA, 49: 270-276, 1966.
4. H.B. Atabek, "End Effects", from "Pulsatile Blood Flow", by E.O. Attinger (Editor), McGraw-Hill Book C., 1964.
5. N.R. Kuchar and S. Ostrach, "Flows in the Entrance Regions of Circular Elastic Tubes", Case Western Reserve University Publication No. FTAS/TR-65-3, Cleveland, 1965.
6. G.S. Malindzak Jr., "Reflection of Pressure Pulses in the Aorta", Medical Research Engineering Vol. 6, Fourth Quarter, 1967.
7. R.H. Cox, "Comparison of Linearized Wave Propagation Models for Arterial Blood Flow Analysis", ASME Publication No. 69-BHF-15, 1969.
8. J.W. Amyot, G.P. Francis, K.M. Kiser, H.L. Falsetti, "Measurement of Sequential Velocity Development in the Aorta", The American Society of Mechanical Engineers (ASME) Winter Annual Meeting, November 29-December 3, 1970, Paper No. 70-WA/BHF-13.
9. D.L. Fry, M.D., A.J. Mallos, B.S. and A.G.T. Casper, B.A. "A Catheter Tip Method for Measurement of the Instantaneous Aortic Blood Velocity", from the Laboratory of Cardiopulmonary Mechanics, Clinic of General Medicine and Experimental Thorapentics, National Heart Institute, Nat. Institutes of Health, U.S. Public Health Service, U.S. Department of Health, Education, and Welfare, Bethesda, Maryland, April 25, 1956.

10. M.P. Spencer, M.D.; and A.B. Denison, M.D.; "The Aortic Flow Pulse as Related to Differential Pressure", The Department of Physiology and Pharmacology, The Bowman Gray School of Medicine, Make Forest College, Winston-Salem, N.C. The Meeting of the American Physiological Society, Atlantic City, New Jersey, April 18, 1956, Circulation Research, Volume I, July 1956.

11. M.F. Snyder, V.C. Rideout, R.J. Hillestand, "Computer Modeling of the Human Systematic Arterial Tree", J. Biomechanics, Vol. I, pp. 341-353, Pergamon Press, 1968, Printed in Great Britain.

12. C.M. Rodkiewicz, and D.H. Howell, "Fluid Dynamics in a Large Arterial Bifurcation", AIAA Journal, Vol. 9, No. 11, Pages 2284-2286, November 1971; See Also Howell, D.H., M.Sc. Thesis, University of Alberta, Edmonton, Alberta, 1968.

13. Hidesato Ito, "Theory on Laminar Flows Through Curved Pipes of Elliptic and Rectangular Cross-sections", The Reports of the Institute of High Speed Mechanics, Tohoku University, Sendai, Japan, December 5, 1950.

14. C.M. Rodkiewicz, and Ch.L. Roussel, "Flow Characteristics in Arterial Junctions", Paper No. 72-WA/FE-8.

15. N.R. Kuchar and S.M. Scala, "Design of Devices for Optimum Blood Flow", ASME Publication No. 68-DE-52, 1968.

16. H. Schlichting, "Boundary Layer Theory", McGraw-Hill Book Co., 1968, Sixth edition.

17. C.M. White, "Streamline Flow Through Curved Pipes", Proc. Roy. Soc. London A 123, 645, 1929.

18. W.R. Dean, "Note on the Motion of Fluid in a Curved Pipe", Phil. Mag., Ser. 7, 4, 1927, 208.

19. W.R. Dean, "The Streamline Motion of Fluid in Curved Pipe, (Second Paper), Phil. Mag., Ser. 7, 5, 1928, 673.

20. M.M. Wintrobe, "Clinical Haematology", Lea and Febiger, Philadelphia, 1968.

21. W.W. Tuttle and B.A. Schottelius, "Textbook of Physiology", The C.V. Mosby Company, St. Louis, 1965.

22. G.H. Bell, and J.N. Davidson, and H. Scarborough, "Textbook of Physiology and Biochemistry", E. and S. Livingstone LTD., Edinburgh and London, 1965, Sixth Edition.

23. A.C. Burton, "Physiology and Biophysics of the Circulation and Introductory Test", Published: Yearbook Medical Publishers Incorporated 35 East Wacker Drive, Chicago, 1968.

24. D.W. Weiting, "A Method of Analyzing the Dynamic Flow Characteristics of Prosthetic Heart Valves", ASME Publication No. 68-WA/BHF-3, 1968.

25. Davis, W., and R.W. Fox, "An Evaluation of the Hydrogen Bubble Technique for the Quantitative Determination of Fluid Velocities Within Clear Tubes", ASME Publication No. 66-WA/PE-21, 1966.

26. PD Dr. E. Strehler, Dr. P. Schmid, "Nomogram for Determining Normal Aortic Diameter (Aortic Arch) and Aortic Biological Age in 2-m Chest X-Rays", Folia Medica Geigy, J.R. Geigy S.A., CH-4000 Basle 18, Switzerland.

APPENDIX A

APPENDIX A

SPECIFIC GRAVITY AND VISCOSITY OF THE BLOOD ANALOGUE

This appendix is a condensation of the detailed studies done by Rodkiewicz-Howell[12], from which the following physical constants have been obtained:

1. The blood analogue used was a mixture of glycerine and water of which 36.7% was glycerine by volume.
2. The specific gravity of glycerine, measured with an Exax Heavy Liquid Hydrometer, was 1.270.
3. The specific gravity of the mixture is as follows:

$$= .367\ (1.270) + .633\ (1.000)$$
$$= .466 + .633$$
$$= 1.099$$

4. The weight percent of glycerine of mixture

$$= \frac{.466}{1.099} = 42.4\%$$

Thus 42.4 lb. of the glycerine and 57.6 lb. of the water were weighted for each 100 lb. mixture. The value 1.1 of the mixture was checked with the Exax Heavy Liquid Hydrometer before each experiment was carried out. This mixture gives a viscosity of the blood analogue of 4.5 centipoise.

APPENDIX B

APPENDIX B

PISTON STROKE CALCULATIONS

The length of the piston stroke was varied by using cams of different sizes, so that the effect of changes in the normalized velocity fluctuation could be studied. The fluctuation component, λ is also dependent on the pulse rate, ω and the flow rate, Q.

The value of λ will change if ω or Q is changed, even though the cam is not changed.

The relationship between Q, ω, λ, and the length of stroke, l is determined as follows:

Consider the instantaneous flow rate simulated on Figure 3.3. It can be described as equal to

$$Q + \frac{Q'}{2} \sin \left(\frac{2\pi}{T_o} t\right) \qquad (B.1)$$

where: Q' is fluctuating component of the flow rate,

T_o is the time required to complete one pulse,

t is the time variable.

Since Q and Q' are directly proportional to the velocity, U, and fluctuating component of velocity, U', it is possible to write

$$\lambda = \frac{Q'}{Q} = \frac{U'}{U}$$

so that

$$Q' = \lambda Q. \qquad (B.2)$$

Therefore, the instantaneous flow rate becomes

$$Q\left[1 + \frac{\lambda}{2} \sin\left(\frac{2\pi}{T_o}\right) t\right]$$

The required swept volume of the piston equals the shaded area of Figure 3.3.

The required swept volume becomes

$$\int_0^{\frac{T_o}{2}} \frac{\lambda Q}{2} \sin\left(\frac{2\pi}{T_o}\right) t \, dt$$

$$= \left[- \frac{\lambda Q}{2} \frac{T_o}{2\pi} \cos \frac{2\pi}{T_o} t \right]_0^{\frac{T_o}{2}}$$

$$= - \frac{\lambda Q}{2} \frac{T_o}{2\pi} \cos\left(\frac{2\pi}{T_o} \frac{T_o}{2}\right) + \frac{\lambda Q}{2} \frac{T_o}{2\pi} \cos \frac{2\pi}{T_o}$$

$$= + \frac{\lambda Q}{2} \frac{T_o}{2\pi} + \frac{\lambda Q}{2} \frac{T_o}{2\pi}$$

$$= \frac{T_o}{2\pi} \lambda Q$$

$$= \frac{\lambda Q T_o}{2\pi} \qquad \text{(B.3)}$$

The time required for one pulse equals the reciprocal of the pulse rate.

Therefore

$$T_o = \frac{1}{\omega} \tag{B.4}$$

Substituting equation (B.4) into equation (B.3), the required swept volume becomes

$$\frac{\lambda Q}{2\pi\omega} \tag{B.5}$$

The required length of stroke is obtained when the volume is divided by the cross-sectional area of the piston (diameter = 4 inches and applying the appropriate conversion factors.

That is,

$$l = \frac{\frac{\lambda Q}{2\pi\omega} \times 61.025\ (\text{inch})^3}{\pi\ (2)^2\ (\text{inch})^2}$$

$$l = 0.77\ \frac{\lambda Q}{\omega}\ (\text{inch}) \tag{B.6}$$

The minimum l was found to be

$$l_{min} = 0.770\ \frac{1 \times 2.85}{115}$$

$$l_{min} = 0.019 \text{ inches}, \tag{B.7}$$

and the maximum l was found to be

$$l_{max} = 0.77 \frac{2 \times 9.84}{28}$$

$$l_{max} = 0.541 \text{ inches.} \qquad \text{(B.8)}$$

APPENDIX C

Table C-4.a

Dependence of Mass Flow Ratios on Re for Steady Flow of Mixture (Glycerine + Water) at a Static Pressure of 115 mm Hg

Re	γ_1	γ_2	γ_3	γ_4	γ_5
370.4	.129	.196	.157	.196	.333
463.0	.132	.181	.155	.190	.356
555.6	.127	.169	.145	.184	.373
648.2	.123	.158	.142	.173	.389
740.8	.126	.157	.138	.176	.410
833.4	.122	.150	.131	.170	.419
926.0	.120	.147	.130	.168	.425
1018.6	.120	.143	.128	.166	.439
1111.2	.117	.141	.122	.168	.448
1203.8	.123	.136	.129	.163	.456
1296.4	.117	.135	.126	.164	.463
1389.0	.114	.133	.125	.161	.476
1481.6	.121	.126	.119	.159	.483
1574.2	.114	.130	.117	.156	.470
1666.8	.116	.128	.119	.157	.476
1759.4	.112	.124	.115	.159	.485
1792.7	.115	.125	.114	.155	.495

Re = 185.2 x Q; Q (liter/min.)

Table C-4.1

Dependence of Mass Flow Ratios on α for Re = 1300 and λ = 1.5

l (ins.)	ω	α	γ_1	γ_2	γ_3	γ_4	γ_5
0.35	23.11	8.58	.118	.137	.124	.167	.465
*0.35	23.11	8.58	.117	.136	.126	.168	.460
0.33	24.51	8.87	.114	.137	.122	.166	.460
0.31	26.09	9.12	.114	.133	.121	.165	.467
0.27	29.96	9.78	.114	.137	.119	.165	.465
*0.27	29.96	9.78	.112	.133	.121	.164	.465
0.25	32.36	10.15	.114	.133	.121	.161	.462
0.23	35.17	10.58	.111	.130	.116	.163	.457
*0.23	35.17	10.58	.112	.130	.120	.165	.465
0.20	40.45	11.37	.113	.128	.122	.163	.467
0.18	44.94	11.97	.112	.131	.118	.163	.472
0.15	53.93	13.10	.111	.130	.122	.165	.475
*0.15	53.93	13.10	.112	.129	.120	.166	.479
0.12	67.41	14.67	.114	.133	.122	.162	.457
0.10	80.90	16.06	.111	.135	.123	.163	.467
0.08	101.12	17.93	.114	.132	.123	.162	.465
*0.08	101.12	17.93	.114	.131	.122	.162	.467
0.07	115.57	19.15	.113	.133	.122	.162	.467

Q = 7.01 liter/min.

Table C-4.2

Dependence of Mass Flow Ratios on

α for Re = 800 and λ = 1

l(ins)	ω	α	γ_1	γ_2	γ_3	γ_4	γ_5
0.15	22.13	8.38	.123	.149	.134	.171	.410
0.14	23.71	8.69	.122	.149	.133	.174	.409
0.13	25.54	9.03	.125	.148	.134	.174	.409
0.12	27.66	9.40	.124	.149	.134	.173	.408
0.11	30.18	9.81	.125	.148	.133	.173	.409
0.10	33.20	10.69	.121	.147	.132	.171	.411
0.09	36.88	10.83	.123	.148	.133	.172	.410
0.08	41.50	11.51	.122	.147	.133	.171	.410
0.07	47.42	12.29	.123	.149	.132	.169	.411
0.06	55.33	13.28	.124	.149	.135	.173	.416
0.05	66.40	14.56	.124	.148	.134	.171	.412
0.04	83.00	16.29	.123	.148	.134	.171	.414
0.03	110.66	19.29	.123	.147	.133	.173	.409

Q = 4.31 liter/min.

Table C-4.3

Dependence of Mass Flow Ratios on

α for Re = 1300 and λ = 1

l(ins)	ω	α	γ_1	γ_2	γ_3	γ_4	γ_5
0.25	21.56	8.30	.114	.131	.126	.165	.452
0.23	23.43	8.63	.108	.134	.118	.165	.466
0.20	26.95	9.28	.112	.129	.120	.162	.457
0.18	29.94	9.78	.110	.131	.120	.161	.457
0.15	35.93	10.71	.110	.132	.121	.162	.462
0.13	41.46	11.49	.114	.133	.124	.163	.464
0.11	49.00	12.49	.114	.132	.123	.162	.460
0.10	53.90	13.14	.115	.135	.123	.161	.469
0.09	59.88	13.83	.116	.134	.125	.162	.460
0.08	67.37	14.67	.115	.133	.123	.162	.462
0.07	77.00	15.69	.115	.135	.124	.162	.460
0.06	89.83	16.93	.114	.133	.122	.161	.460
0.05	107.80	17.92	.115	.133	.122	.162	.460
0.04	134.70	20.74	.115	.133	.124	.162	.462

Q = 7.01 liter/min.

Table C-4.4

Dependence of Mass Flow Ratios on

α for Re = 1800 and λ = 1

l(ins)	ω	α	γ_1	γ_2	γ_3	γ_4	γ_5
0.35	21.30	8.24	.114	.126	.117	.162	.475
*0.35	21.30	8.24	.113	.127	.119	.158	.471
0.33	22.65	8.51	.113	.125	.122	.164	.475
0.31	24.11	8.78	.110	.126	.119	.160	.475
0.27	27.69	9.40	.107	.124	.112	.162	.483
*0.27	27.69	9.40	.108	.126	.116	.159	.471
0.25	29.90	9.78	.107	.127	.117	.160	.482
0.23	32.50	10.37	.107	.124	.115	.160	.486
*0.23	32.50	10.37	.108	.122	.117	.159	.486
0.20	37.38	10.90	.107	.124	.110	.156	.475
0.18	41.54	11.51	.107	.123	.114	.158	.482
0.15	49.84	12.62	.106	.123	.112	.160	.490
*0.15	49.84	12.62	.107	.123	.111	.159	.493
0.12	62.30	14.10	.111	.124	.116	.156	.475
0.10	74.76	15.46	.109	.127	.118	.162	.482
0.08	93.46	17.26	.110	.126	.117	.159	.478
*0.08	93.46	17.26	.110	.124	.116	.158	.482
0.06	124.61	19.99	.108	.125	.114	.156	.478

Q = 9.71 liter/min.

Table C-4.5

Dependence of Mass Flow Ratios on Re

for $\alpha = 10$ and $\lambda = 1$

l(ins)	Q(l.p.m.)	Re	γ_1	γ_2	γ_3	γ_4	γ_5
0.23	9.37	1736	.107	.126	.117	.158	.457
*0.23	9.37	1736	.109	.127	.116	.159	.470
0.20	8.15	1509.5	.112	.132	.119	.161	.462
0.18	7.33	1358	.113	.131	.121	.162	.462
*0.18	7.33	1358	.112	.133	.122	.164	.457
0.15	6.11	1132	.113	.136	.122	.166	.450
0.14	5.70	1056	.116	.141	.124	.170	.445
0.13	5.39	981	.116	.140	.125	.165	.424
0.12	4.88	905	.117	.144	.132	.170	.420
0.11	4.48	830	.118	.149	.129	.167	.418
*0.11	4.48	830	.121	.148	.133	.169	.429
0.10	4.07	755	.124	.153	.133	.176	.418
*0.10	4.07	755	.119	.150	.132	.173	.421
0.09	3.66	679	.128	.159	.139	.176	.400
*0.09	3.66	679	.123	.157	.137	.176	.405
0.08	3.25	604	.127	.160	.138	.183	.387
*0.08	3.25	604	.123	.164	.140	.186	.391
0.07	2.85	528	.129	.169	.144	.181	.368
*0.07	2.85	528	.118	.171	.145	.189	.350

$\omega = 31.38$ revolutions/min.

Table C-4.6

Dependence of Mass Flow Ratios on Re

for $\alpha = 10$ and $\lambda = 1.5$

l(ins)	Q(l.p.m.)	Re	γ_1	γ_2	γ_3	γ_4	γ_5
0.38	10.32	1912	.115	.128	.119	.161	.476
0.36	9.78	1811.4	.106	.126	.116	.162	.471
0.35	9.50	1761	.110	.129	.120	.163	.451
0.34	9.24	1710.7	.108	.128	.117	.163	.470
0.33	8.96	1660	.111	.129	.117	.160	.471
0.32	8.69	1610.1	.112	.129	.117	.160	.469
0.31	8.42	1560	.109	.129	.119	.164	.471
0.27	7.33	1358.5	.112	.134	.122	.165	.475
0.25	6.79	1258	.112	.130	.120	.166	.453
*0.25	6.79	1258	.114	.133	.123	.167	.464
0.23	6.24	1157	.109	.139	.121	.162	.451
*0.23	6.24	1157	.113	.139	.122	.166	.457
0.20	5.43	1006	.113	.143	.130	.171	.445
0.18	4.89	906	.114	.141	.126	.172	.434
*0.18	4.89	906	.116	.144	.128	.171	.436
0.15	4.07	755	.113	.147	.126	.177	.424
*0.15	4.07	755	.113	.148	.129	.174	.430
0.14	3.80	704	.120	.153	.129	.171	.397
*0.14	3.80	704	.114	.150	.130	.170	.415
0.13	3.53	654	.124	.155	.137	.175	.404
*0.13	3.53	654	.120	.154	.136	.175	.402
0.12	3.25	604	.130	.162	.139	.179	.384
0.11	2.98	553	.121	.168	.140	.186	.418
*0.11	2.98	553	.121	.166	.140	.186	.406
0.10	2.71	503	.128	.167	.144	.184	.386
*0.10	2.71	503	.124	.170	.145	.186	.389

$\omega = 31.38$ revolutions/min.

Table C-4.7

Dependence of Mass Flow Ratios on Re for

$\alpha = 10$ and $\lambda = 2$

l(ins)	Q(l.p.m)	Re	γ_1	γ_2	γ_3	γ_4	γ_5
0.47	9.57	1773.6	.108	.125	.120	.165	.482
0.46	9.37	1736	.113	.129	.118	.166	.467
0.45	9.17	1698.2	.110	.126	.118	.168	.477
0.44	8.96	1660	.113	.123	.121	.162	.470
0.43	8.76	1622.7	.110	.128	.118	.164	.472
0.42	8.55	1585	.111	.131	.123	.164	.474
0.40	8.15	1509	.113	.131	.120	.163	.465
0.38	7.74	1434	.113	.131	.121	.166	.464
0.35	7.13	1320	.116	.138	.120	.171	.467
0.33	6.72	1245	.110	.135	.122	.167	.469
0.32	6.52	1207.6	.112	.138	.122	.170	.464
0.31	6.31	1170	.115	.133	.119	.166	.458
0.27	5.50	1019	.111	.136	.121	.167	.436
0.25	5.09	943	.112	.128	.122	.172	.436
*0.25	5.09	943	.114	.132	.126	.166	.441
0.23	4.68	868	.107	.137	.122	.170	.433
0.18	3.66	679	.113	.148	.130	.175	.409
0.15	3.05	566	.110	.158	.128	.184	.402
*0.15	3.05	566	.114	.154	.133	.180	.413
0.14	2.85	528	.113	.164	.137	.189	.412
*0.14	2.85	528	.115	.161	.137	.188	.413
0.13	2.64	490	.123	.171	.144	.183	.361
*0.13	2.64	490	.121	.166	.146	.185	.384

$\omega = 31.38$ revolutions/min.

Table C-4.8

Dependence of Mass Flow Ratios on Re

for $\alpha = 15$ and $\lambda = 2$

l(ins)	Q(l.p.m)	Re	γ_1	γ_2	γ_3	γ_4	γ_5
0.20	9.17	1698	.107	.123	.114	.161	.484
*0.20	9.17	1698	.110	.125	.112	.158	.491
0.18	8.25	1528	.111	.129	.118	.161	.478
*0.18	8.25	1528	.111	.188	.119	.161	.475
0.15	6.87	1274	.109	.132	.124	.161	.457
0.13	5.96	1104	.116	.136	.126	.166	.470
0.12	5.50	1019	.115	.137	.125	.163	.431
0.11	5.04	934	.120	.142	.132	.168	.440
*0.11	5.04	934	.118	.142	.128	.171	.434
0.10	4.58	849	.117	.142	.126	.166	.433
*0.10	4.58	849	.120	.144	.129	.173	.433
0.09	4.12	764	.122	.150	.134	.174	.413
*0.09	4.12	764	.117	.153	.134	.178	.418
0.08	3.66	679	.124	.156	.139	.176	.393
*0.08	3.66	679	.125	.159	.140	.175	.390
0.07	3.21	594	.126	.163	.137	.180	.370
*0.07	3.21	594	.124	.163	.140	.182	.376
0.06	2.75	509	.130	.172	.148	.183	.364
*0.06	2.75	509	.130	.173	.152	.184	.376

$\omega = 70.62$ revolutions/min.

Table C-4.9

Dependence of Mass Flow Ratios on Re

for $\alpha = 19$ and $\lambda = 2$

l(ins)	Q(l.p.m)	Re	γ_1	γ_2	γ_3	γ_4	γ_5
0.14	10.30	1907	.110	.119	.114	.151	.510
0.13	9.56	1771	.114	.120	.113	.153	.482
0.12	8.82	1635	.113	.127	.116	.157	.474
0.11	8.09	1498	.109	.126	.117	.159	.480
0.10	7.35	1361	.114	.128	.115	.160	.469
*0.10	7.35	1361	.110	.128	.116	.161	.485
0.09	6.62	1226	.118	.134	.124	.164	.464
*0.09	6.62	1226	.116	.134	.123	.168	.467
0.08	5.88	1090	.120	.138	.122	.164	.463
*0.08	5.88	1090	.116	.135	.123	.168	.468
0.07	5.15	954	.120	.141	.128	.180	.431
*0.07	5.15	954	.116	.139	.127	.172	.439
0.06	4.41	817	.119	.149	.131	.170	.418
*0.06	4.41	817	.121	.148	.131	.170	.426
0.05	3.67	681	.117	.151	.131	.178	.419
*0.05	3.67	681	.122	.150	.129	.176	.416
0.04	2.94	545	.126	.172	.146	.181	.377
*0.04	2.94	545	.126	.172	.151	.187	.375
0.03	2.20	409	.133	.193	.157	.195	.387
*0.03	2.20	409	.129	.185	.155	.191	.340

ω = 113.3 revolutions/min.

APPENDIX D

APPENDIX D

ROTAMETER CALIBRATION

The calibration results for the rotameter are shown in Figure D.1. The curve obtained is in linear; the volume rates for intermediate rotameter readings are obtained by interpolation.

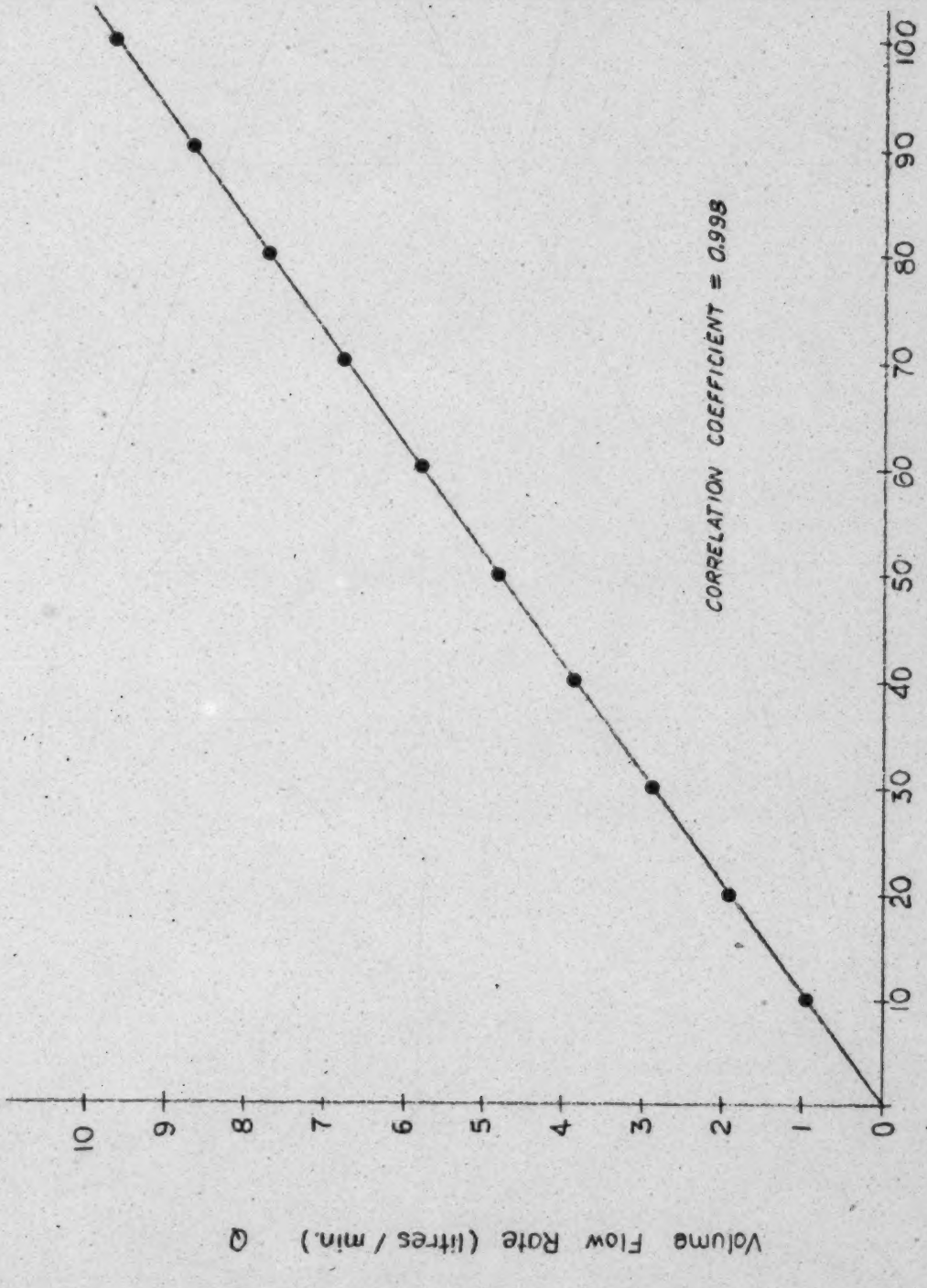

Figure D.1: Rotameter Calibration Characteristics.